Do all chlorophyll fluorescence emission wavelengths capture the spring recovery of photosynthesis in boreal evergreen foliage?

Running title: Spectral fluorescence in evergreens

Chao Zhang[1, 2, 3, *], Jon Atherton[1], Josep Peñuelas[2, 3], Iolanda Filella[2, 3], Pasi Kolari[4], Juho Aalto[4, 5], Hanna Ruhanen[6], Jaana Bäck[7], Albert Porcar-Castell[1,*]

[1]Optics of Photosynthesis Laboratory, Institute for Atmospheric and Earth System Research (INAR)/Forest Sciences/Viikki Plant Science Centre, Faculty of Agriculture and Forestry, University of Helsinki, PO Box 27, 00014 Helsinki, Finland.

[2]CREAF, Center for Ecological Research and Forestry Applications, Bellaterra 08193, Catalonia, Spain.

[3]CSIC, Global Ecology Unit CREAF-CSIC-UAB, Cerdanyola del Vallès 08193, Catalonia, Spain

[4]Department of Physics, University of Helsinki, PO Box 64, 00014 Helsinki, Finland.

[5]SMEAR II Station, University of Helsinki, Hyytiäläntie 124, Korkeakoski 35500, Finland

[6]Natural Resources Institute Finland (Luke), Natural Resources and Bioproduction, Suonenjoki Unit, Juntintie 154, 77600 Suonenjoki, Finland.

[7]Department of Forest Sciences, University of Helsinki, PO Box 27, 00014 Helsinki, Finland.

*Corresponding authors: Chao Zhang, chao.x.zhang@helsinki.fi; Albert Porcar-Castell, joan.porcar@helsinki.fi

Abstract

Chlorophyll *a* fluorescence (ChlF) is closely related to photosynthesis and can be measured remotely using multiple spectral features as solar-induced fluorescence (SIF). In boreal regions, SIF shows particular promise as an indicator of photosynthesis; in part because of the limited variation of seasonal light absorption in these ecosystems. Seasonal spectral changes in ChlF could yield new information on processes such as sustained non-photochemical quenching (NPQ_S), but also disrupt the relationship between SIF and photosynthesis. We followed ChlF, functional and biochemical properties of *Pinus sylvestris* needles during the photosynthetic spring recovery period to answer; (1) how ChlF spectra change over seasonal timescales? (2) How pigments, NPQ_S and total PAR absorption drive changes of ChlF spectra? (3) Do all ChlF wavelengths track photosynthetic seasonality? We found seasonal ChlF variation in the red and far-red wavelengths, which was strongly correlated with NPQ_S, carotenoid content and photosynthesis (enhanced in the red), but not with PAR absorption. Furthermore, a rapid decrease in red/far-red ChlF ratio occurred in response to a cold spell, potentially relating to the structural reorganization of the photosystems. We conclude that all current SIF retrieval features can track seasonal photosynthetic dynamics in boreal evergreens, but the full SIF spectra provides additional insight.

Key words: chlorophyll *a* fluorescence spectra, evergreen vegetation, F_{690}, F_{740}, leaf PAR absorption, *Pinus sylvestris*, PSI fluorescence, fluorescence ratio, sustained non-photochemical quenching (NPQ_S)

Introduction

Chlorophyll *a* fluorescence (ChlF) of leaves, thylakoids and photosystems has been extensively used to study the organization, functioning, and acclimation of the photosynthetic light harvesting apparatus (Govindjee 1995; Baker 2008; Murchie & Lawson 2013; Porcar-Castell *et al.* 2014). ChlF can now be measured within discrete wavelengths from plant canopies, forest stands, and whole ecosystems with instrumentation on towers, drones, aircraft and satellites (Zarco-Tejada, Catalina, González & Martín 2013; Porcar-Castell *et al.* 2015; Rascher *et al.* 2015; Joiner, Yoshida, Guanter & Middleton 2016; Sun *et al.* 2017; Parazoo *et al.* 2018). Widely addressed as solar-induced fluorescence (SIF) by the remote sensing community, SIF opens up the study of photosynthesis at unprecedented scales (Frankenberg *et al.* 2011, 2014; Parazoo *et al.* 2014; Thum *et al.* 2017; Sun *et al.* 2018; Zhang, Guanter, Joiner, Song & Guan 2018; Zuromski *et al.* 2018). This capacity could not only serve to improve the current accuracy of global carbon budgets (Damm *et al.* 2015; Quéré *et al.* 2018; Smith *et al.* 2018) but yield new understanding on the responses and feedbacks between terrestrial ecosystems and the environment, both critical milestones for the implementation of climate change mitigation and adaptation strategies (Smith *et al.* 2014; IPCC-SR15 2018).

Despite the mounting evidence of the strong link between SIF and gross primary productivity (GPP) accumulating from ground, airborne and satellite platforms (Guanter *et al.* 2014; Zarco-Tejada, González-Dugo & Fereres 2016; Migliavacca *et al.* 2017; Sun *et al.* 2017; Parazoo *et al.* 2018; Zuromski *et al.* 2018; Magney *et al.* 2019a), the physical and biological mechanisms that underpin the relationship and the potential wavelength-dependent information content in the

SIF signal remain unclear (Porcar-Castell *et al.* 2014; Verrelst *et al.* 2016; Wieneke *et al.* 2018; Yang *et al.* 2018). This lack of understanding, is particularly acute for evergreen foliage, where the seasonal link between SIF and GPP involves processes other than changes in absorbed photosynthetically active radiation(APAR) which could decouple and add wavelength dependencies to the relationship between SIF and GPP.

In contrast to pulse-amplitude-modulation (PAM) ChlF measurements which integrate ChlF over a broad range of wavelengths, SIF is retrieved within narrow and discrete spectral bands around the red and far-red ChlF emission peaks (atmospheric oxygen absorption bands or solar Fraunhofer lines) (Alonso *et al.* 2007; Meroni *et al.* 2009). Accordingly, because the shape of the leaf-level ChlF spectra is driven by a combination of physical, physiological and biochemical factors (Magney *et al.* 2019b), it can be expected that the seasonal relationship between SIF and GPP would depend on retrieval wavelength, especially in boreal evergreen vegetation undergoing remarkable adjustments during the season.

A light use efficiency type model (Monteith 1972) becomes a convenient theoretical framework to introduce the physical and biological factors that couple (or decouple) SIF and GPP, and connect the leaf-level phenomenology to the spatial scale of remote sensing. The intensity of the SIF signal emitted from a leaf or a plant canopy at a given wavelength (λ) can be expressed as a function of four factors: 1) the incoming PAR, 2) the fraction of that PAR absorbed by the leaf or canopy (A), 3) the quantum yield of fluorescence with its associated emission wavelength ($\Phi_F(\lambda)$), and 4) a wavelength dependent escape probability ($f_{esc}(\lambda)$) which accounts for the reabsorption of predominantly red ChlF photons by chlorophyll (Chl) molecules within the antenna, thylakoid, chloroplast, leaf or

plant canopy (Buschmann 2007; Porcar-Castell *et al.* 2014; Romero, Cordon & Lagorio 2018; Yang & van der Tol 2018), as:

$$SIF(\lambda) = PAR \cdot A \cdot \Phi_F(\lambda) \cdot f_{esc}(\lambda) \quad \text{(Eqn. 1)}$$

In similar terms, leaf or canopy level GPP can be expressed as:

$$GPP = PAR \cdot A \cdot LUE \quad \text{(Eqn. 2)}$$

where LUE corresponds to the photosynthetic light use efficiency in moles of CO_2 assimilated moles per mole of absorbed PAR photons. By combining equations (note that *A* and PAR cancel out), a simple theoretical relationship that links GPP to SIF can be obtained as:

$$GPP = \frac{1}{f_{esc}(\lambda)} \cdot \frac{LUE}{\Phi_F(\lambda)} \cdot SIF(\lambda) \quad \text{(Eqn. 3)}$$

In this equation, widely applied to the interpretation of remotely sensed SIF data (Guanter *et al.* 2014; van der Tol, Berry, Campbell & Rascher 2014; Damm *et al.* 2015; Lee *et al.* 2015; Frankenberg & Berry 2018), physical factors (e.g. structure-dependent ChlF reabsorption) are embedded in the $1/f_{esc}(\lambda)$ term, and biological factors (e.g. architecture and physiological state of the light reactions, alternative energy sinks, cyclic electron transport, photorespiration) are embedded in the $LUE/\Phi_F(\lambda)$ term. Clearly, any seasonal changes in the strength of the factors above can potentially couple and decouple SIF and GPP (Porcar-Castell *et al.* 2014). In addition, any seasonal changes in the leaf-level wavelength properties of $f_{esc}(\lambda)$ and $\Phi_F(\lambda)$ can add wavelength dependencies to the link between SIF(λ) and GPP, something that remains to be characterized.

Seasonal changes in leaf Chl content, although usually modest in boreal evergreens (Öquist & Huner 2003; Ensminger *et al.* 2004; Porcar-Castell *et al.*

2008a), affect light absorption, and also $f_{esc}(\lambda)$ via ChlF reabsorption (Buschmann 2007). Similarly, structural changes at the level of chloroplast and thylakoid membrane, e.g. thylakoid grana unstacking and aggregation of Chl binding light harvesting complexes in overwintering evergreens (Öquist, Chow & Anderson 1992; Ruban, Johnson & Duffy 2012; Verhoeven 2014; Demmig-Adams, Muller, Stewart, Cohu & Adams 2015; Ruban 2016) could also contribute to the modulation of $f_{esc}(\lambda)$ potentially affecting the spectral properties of SIF and its seasonal correlation to GPP.

$\Phi_F(\lambda)$ is composed of at least two components: a highly dynamic component which responds to photochemical (PQ) and non-photochemical (NPQ) quenching of excitation energy in photosystem II (PSII) and that fluoresces in the red and far-red regions (Franck, Juneau & Popovic 2002; Palombi *et al.* 2011), and a component from photosystem I (PSI) assumed to remain stationary over the short term (Genty, Wonders & Baker 1990; Palombi *et al.* 2011; Pfündel, Klughammer, Meister & Cerovic 2013) that fluoresces predominantly in the near-infrared. Accordingly, if seasonal dynamics in sustained NPQ (NPQ_S) (Ottander, Campbell & Öquist 1995; Öquist & Huner 2003; Verhoeven 2014) quenched only the ChlF components from PSII, one would expect NPQs to affect the spectral properties of $\Phi_F(\lambda)$. Similarly, differences in the patterns of seasonal photoinhibition of PSII (Ensminger *et al.* 2004; Murata, Takahashi, Nishiyama & Allakhverdiev 2007) and PSI reaction centres (Sonoike 2011; Huang, Yang, Hu & Zhang 2016) could also affect the ChlF spectra and its spectral dependency with photosynthesis.

In summary, although a strong seasonal coupling between PAM ChlF and photosynthesis has been widely reported for evergreen foliage (e.g. Ottander & Öquist 1991; Ensminger *et al.* 2004; Zarter, Demmig-Adams, Ebbert, Adamska

148 & Adams 2006b; Soukupová *et al.* 2008; Kolari *et al.* 2014; Springer, Wang &
149 Gamon 2017), the spectral dependency of the relationship remains unresolved.

150 The objective of the study was to characterize the seasonal variation of ChlF
151 spectra for boreal evergreen Scots pine needles during the spring recovery of
152 photosynthesis. Hence, we investigated if red and far-red wavelengths of ChlF
153 were equally positioned to capture the spring recovery of photosynthesis. To do
154 so we combined long-term and continuous *in situ* measurements of gas exchange,
155 and PAM ChlF with repeated measurements of foliar pigment content, leaf total
156 PAR absorption and spectral ChlF, spanning the full dynamic range of variation
157 in photosynthetic capacity of Scots pine needles: from deeply downregulated
158 foliage during winter, to fully functional foliage during peak growing season in
159 summer**.**

160

161 **Materials and methods**

162 *Study site and field sampling protocol*

163 Measurements were conducted at Hyytiälä/SMEAR-II (Station for Measuring
164 Forest Ecosystem-Atmosphere Relations) in Southern Finland (61°51´N,
165 24°17´E, 181m a. s. l.) (Hari & Kulmala 2005), in a 52-year old Scots pine (*Pinus*
166 *sylvestris* L.) stand with a dominant height of c. 18m. The study period (24th
167 February - 20th July 2015) encompassed three biological seasons: end of winter
168 (full dormant state), spring, and first half of summer (peak growing season).

169 The study combined continuous *in situ* measurements of micrometeorological
170 variables, CO_2 exchange and PAM ChlF across four different trees (N= 4), with
171 repeated point measurements of steady-state spectral ChlF at room temperature

and pigment analysis across five trees (previous four plus one, N=5). Spectral ChlF was purposefully measured under standardized PAR so that it could serve as a proxy of $\Phi_F(\lambda)$ in Eqns 1 and 3, (i.e. APAR assumed constant). To avoid changing the needle cohort in the middle of the experiment, all measurements were conducted in the newest cohort of needles available at the start of the study period (developed in summer 2014). To avoid defoliation effects, several branches from the four topmost whorls were selected per tree and used for the repeated sampling of needles. Needles were sampled always before 10AM. Overall, the study included a total of 19 measuring points in addition to the continuous measurements (Fig. 1).

Continuous measurements of micrometeorological data and shoot CO_2 exchange

Air temperature (°C) (Pt100 sensor) and PAR (µmol m^{-2} s^{-1}) (Li-190SZ, Li-Cor Inc., Lincoln, NE, USA) were measured right above the forest at 1 min intervals from sensors placed in a tall mast. The CO_2 exchange of pine shoots was measured in top canopy shoots 30-60 times per day using a system of automated dynamic chambers coupled to an infrared gas analyzer (Li-840, Li-Cor Inc., Lincoln, NE, USA) (see e.g. Aalto *et al.* 2014 for further details). Chambers remained open most of the time exposing the studied shoots to ambient conditions and closed only during measurement. Fluxes were estimated from the change in CO_2 concentration during the first 40 s upon chamber closure (Kolari *et al.* 2012). Shoots with fully developed needles from 2014 were debudded prior to chamber installation to prevent new growth during the study period and for practical reasons. Total needle area inside the chamber was measured at the end of the study and used to calculate fluxes. A total of two to four chambers

(N=2-4) were used during the study period from February 24th to July 20th in 2015 (Fig. S1a).

Direct comparison of noon LUE from chamber data (moles CO_2 assimilated /moles PAR absorbed) can be problematic in boreal conditions due to low PAR levels during the winter months. Accordingly, we decided to use here a simple model of photosynthesis (the optimal stomatal control model) (Hari, Mäkelä, Korpilahti & Holmberg 1986; Kolari, Lappalainen, Hänninen & Hari 2007) that allows robust estimation of photosynthetic parameters under ambient CO_2 concentrations, low light and low temperatures (Kolari *et al.* 2014). Two key photosynthetic parameters were estimated in a 3-day time window to capture the seasonal development in LUE; (1) α (µmol CO_2 / µmol PAR), the slope of a linear function fitted to the photosynthetic light response with low incident PAR (<300 µmol m^{-2} s^{-1}) before noon (Fig. S1b; Kolari *et al.* 2014). Under constant leaf PAR absorption (Fig. S2), this parameter can be considered a measure of maximum photosynthetic LUE under low light. In addition, and since our spectral ChlF measurements were not conducted under low light, we also estimated (2) β (m s^{-1}), the maximum rate of light-saturated photosynthesis per unit inter-cellular CO_2 concentration (Fig. S1c). This parameter can be considered a measure of light-saturated photosynthesis at optimal temperature, low vapour pressure deficit and ambient CO_2 concentration.

We normalized α and β parameters to their mean values between May 3rd and 23rd (see Fig. S1d,e). This is a common procedure in time-series analysis and serves to minimize the impact of systematic variability and emphasize the seasonal patterns in the data, which was our goal. The normalization period was selected in May as that was the time when all four chambers were simultaneously

recording and the foliage was already photosynthetically active. Normalized unitless values were then converted back to the original units by multiplying the normalized values by the respective means across all four chambers. The parameters α and β are used hereinafter as a measure of the seasonal spring recovery of photosynthesis.

Continuous measurements of PAM ChlF in situ

A Monitoring PAM system (MONI-PAM, Walz GmbH, and Germany) (Porcar-Castell, Pfündel, Korhonen & Juurola 2008b; Porcar-Castell 2011), equipped with 4 independent PAM fluorometers, was used to record the instantaneous fluorescence yield (F'), the maximal fluorescence yield (F'_M), incoming PAR, and temperature every 30 minutes. Night F' and F'_M were assumed to correspond to minimal (F_o) and maximal (F_M) fluorescence and used to derive daily maximum quantum yield of PSII, F_V/F_M after Kitajima & Butler (1975), and to calculate quenching parameters NPQ_S and PQ_S after Porcar-castell (2011) as: $NPQ_S = F_{MR}/F_M - 1$ and $PQ_S = F_{MR}/F_o - F_{MR}/F_M$, where F_{MR} is the summer night reference obtained for those particular needles in the absence of NPQ_S. A decrease in PQ_S relative to summer levels was here interpreted in terms of photoinhibition of reaction centres (Porcar-Castell 2011). Finally, seasonal changes in PAM based fluorescence yield (Φ_F) were estimated as $\Phi_F = 0.1\ F_o/F_{MR}$ (Porcar-castell 2011, note the unfortunate typo in Eqn. 24 therein where F'_M should be F_{MR}), which is based on the assumption of a maximum fluorescence yield of 10% for PSII particles at the F_M state (Barber, Malkin & Telfer 1989). The four fluorometers were installed in top canopy branches pointing south.

246 *Validation of ChlF measurements*

247 For practical reasons, this study compared ChlF spectra of cut needles measured
248 under standard conditions and at room temperature, with photosynthetic
249 parameters (α, β, F_V/F_M, NPQ_S and PQ_S,) obtained from the field instrumentation.
250 Accordingly, we wanted to test that our measurements at room temperature
251 correctly represented the same physiological state as measurements carried out
252 in the field. In addition, we wanted to ensure that our MONI-PAM system (which
253 consistently supplied 48 light pulses per day to the same needles throughout the
254 study period) was not introducing any long-term artefact. We used a Hansatech
255 fluorometer (FMS-2, Hansatech Instruments Ltd., Kings Lynn, Norfolk, UK) to
256 measure F_V/F_M both in the field and under standardized conditions indoors.
257 During each sampling point, we placed a total of 25 dark-acclimation clips,
258 distributed across the five study trees, and dark acclimated for at least 1 hour
259 prior to measuring F_V/F_M. The same measurements were subsequently repeated
260 at room temperature using collected needles instead. As expected, F_V/F_M
261 obtained from the FMS-2 in the field was highly correlated with estimates from
262 the MONI-PAM system (r=0.97, P<0.0001) (Fig. S3), denoting that the MONI-
263 PAM system did not introduce any bias into the observed seasonal patterns. The
264 small discrepancy between slopes is very likely due to differences in the colour
265 of the measuring light as well as the ChlF detection range between instruments.
266 Similarly, F_V/F_M measurements obtained with the FMS-2 fluorometer in field were
267 found to be strongly correlated with those of detached needles at room
268 temperature (r=0.94, P<0.0001) (Fig. S3), suggesting that room temperature
269 measurements did not introduce any major bias into the observed seasonal
270 patterns in spectral ChlF.

Estimation of foliar pigment content

During each sampling point, five pairs of needles were randomly detached per each tree using the pre-selected top branches and needle cohort. Needles were sampled into cryotubes, immediately frozen at liquid nitrogen temperature using a portable dewar (CX-100, Taylor Wharton International LLC, Minnetonka, MN), and subsequently stored at -80 °C until extraction. Pigment analysis were conducted following Wellburn (1994) with dimethyl sulfoxide (DMSO; VWR Chemicals, 23500.322) as solvent. Frozen samples (75-100 mg) were first homogenized for 2 minutes at 30 Hz, using a bead mill (TissueLyser II Qiagen, Germany), stainless steel beads (4 mm) and microtubules (2 mL). Subsequently, 1.8 mL of DMSO was added to the homogenate and resuspended again at 30 Hz for 1 minute. Pigments were extracted in oven at 40 °C for 4 hours. Extracts were then centrifuged at 25000g for 5 minutes. Light absorption was measured at 649.1 nm, 665.1 nm and 480.0 nm, with a spectrophotometer (Shimadzu UV-2401 PC), and subsequently used for estimation of Chl a, Chl b and total carotenoids (Wellburn 1994).

Measurements of leaf absorption

Needle PAR absorption ($A_{T(PAR)}$) was measured 8 times during the study period (N=5 biological replicates). We used the same spectrometer and LED light source described above connected to a 6 inch diameter integrating sphere (AdaptaSphere, LabSphere Inc, New Hampshire, UK), and applied the black spray method (Olascoaga, Mac Arthur, Atherton & Porcar-Castell 2016) to estimate $A_{T(PAR)}$. The black spray method was inspired by earlier within-sphere measurements (Öquist, Hällgren & Brunes 1978; Idle & Proctor 1983) and

296 purposefully developed to measure absorption in leaves with complex geometry,
297 like needles, because it does not require mounting needles in the port of the
298 integrating sphere and therefore there are no gap effects. Instead, samples are
299 placed inside the sphere and hung from a white thread across the central plane
300 (see illustrations in Olascoaga *et al.* 2016 for details). Prior to measurements, 5-
301 6 needle pairs were separated and the resulting 10-12 needles sewed with a
302 white thread and spaced at least 1 cm. The method consisted of three separate
303 spectral measurements inside the sphere: 1) white thread alone (reference zero
304 absorption, I_W), 2) white thread with needles (sample absorption, I_S), and 3) white
305 thread with needles painted with a black spray of known absorption (Black sample,
306 I_B). Conveniently, because the total surface area of the needles in steps 2) and
307 3) can be assumed to remain constant, this parameter cancels out and there is
308 no need to estimate it. Total PAR absorption can then be computed by combining
309 these three measurements with the known absorption of the black spray (A_{BLACK}),
310 as:

311 $$A_T = \frac{(I_W - I_S)\, I_B\, A_{BLACK}}{(I_W - I_B)\, I_S} \qquad \text{Eqn. 4}$$

312 The mean value of A_T between 400 and 700nm was here used as an estimate of
313 $A_{T(PAR)}$.

314

315 *Room temperature measurements of leaf spectral ChlF*

316 Leaf spectral ChlF (F_{λ}, in mW m^{-2} sr^{-1} nm^{-1}) was measured at room temperature
317 using a FluoWat Clip (Image Processing Laboratory, University of Valencia,
318 Spain) (Van Wittenberghe, Alonso, Verrelst, Moreno & Samson 2015) coupled
319 with a powerful white LED (MJ-858, Magicshine, UK) and a radiometrically

320 calibrated visible-near-infrared spectrometer (FieldSpec, ASD-Panalytical,
321 Boulder, CO). The spectrometer covers the spectral range between 325 and 1075
322 nm at a sampling interval of 1 nm and with a FWHM of 3.5 nm. The FluoWat clip
323 has an optical window for input illumination (incidence angle of 45°) and a small
324 aperture (at nadir view) to connect the optical fiber. The fiber field of view is 25°
325 and the distance to sample is 1 cm, yielding an approximately circular target area
326 of 0.22 cm radius. To obtain spectral ChlF, a 650 nm short-pass filter (Edmund
327 Optics Ltd, UK, OD=4) was used to exclude 99.99% of radiation above 650 nm.
328 The LED source supplies a PAR of c. 1200 µmol at the leaf surface as estimated
329 with a PAR sensor (Licor LI150-A, Li-Cor Inc., Lincoln, NE, USA).

330 Needles were carefully arranged alongside each other to minimize the gap
331 fraction and fixed with transparent tape to conform a needle mat (see Fig. 1).
332 Rajewicz, Atherton, Alonso & Porcar-Castell (2019) recently compared the ChlF
333 spectra of needles with different arrangements, and concluded that despite the
334 fact that needle mats could slightly enhance reabsorption, they provided a higher
335 replicability and reproducibility and were therefore a good solution to track
336 temporal changes in spectral properties.

337 Needle mats were dark adapted at 10 °C for 1 hour and kept in the dark until
338 measurements started in the FluoWat clip. After conducting a dark current
339 measurement, the needle mat was placed in the FluoWat clip, recording was
340 started, and an opaque aluminium foil placed between the light source and the
341 FluoWat clip rapidly removed. Variations of spectral ChlF were recorded during
342 two minutes at an integration time of 136 ms. The last ten spectra were averaged
343 and used to estimate steady-state ChlF between 650 nm and 850 nm (F_λ).
344 Averaged spectra were further smoothed using a Savitzky-Golay filter (order=2,

345 averaging interval=15) and cut to a range of 660-780 nm where the signal was
346 strongest. The resulting fluorescence spectra was used to estimate red (F_{690}) and
347 far-red ChlF (F_{740}) and used to calculate an integrated steady-state ChlF between
348 660 and 780 nm ($\int_{660}^{780} F\, d\lambda$) for correspondence with the broadband PAM
349 fluorescence parameter, Φ_F.

350

351 *Statistical analyses*

352 Mean values of four (gas exchange and Monitoring PAM fluorescence) or five (all
353 other data) trees were used to conduct statistical analysis. Linear regression
354 models and simple Pearson's correlation analyses were used to assess
355 relationships between variables. All the analyses were conducted with R version
356 3.2.2 (R Core Development Team, 2015) and MATLAB version R2014a
357 (MathWorks Inc. 2014).

358 Principal Component Analysis (PCA) was used to quantitatively assess the
359 relative role of different components of variation in the spectral ChlF dataset. In
360 particular, we wanted to quantify how much of the seasonal variation in spectral
361 ChlF during the spring recovery of photosynthesis was related to principal
362 components associated with changes in the intensity and how much was related
363 to principal components associated with changes in the shape. The R function
364 'prcomp' in the default mode ('prcomp' arguments; scale = FALSE and center =
365 TRUE) was used to run a PCA on time series of the ChlF data-set. The analysis
366 was focused on the 660-780 nm emission region to reduce impact of low signal-
367 to-noise at wavelength limits.

368

Results

Seasonal changes in micrometeorological variables and photosynthetic parameters

Both temperature and PAR followed the typical annual pattern in boreal regions with PAR increasing faster and earlier than temperature (Fig. 2a). Daily mean temperatures in February (-1.7 °C) and March (0.6 °C) were higher by 6 and 4 °C, respectively, compared to the average for the period 1981-2010 (Pirinen *et al.* 2012). Fortunately, a cold spell took place on March 22nd with a daily mean temperature of -5.7 °C. On April 16th, a second cold spell took place with a mean temperature of 0.7 °C. These cold spells served to assess the responses of ChlF and photosynthetic parameters to a sudden decrease in temperature and were highlighted in figures reporting the time series.

Noon mean CO_2 fluxes (Fig. 2b) registered a clear seasonal pattern gradually increasing from April to June. Both α (a measure of maximum LUE under low light) and β (a measure of maximum photosynthetic rate) displayed similar seasonal patterns (Fig. 2c), gradually increasing from winter to summer. The effect of the cold spells on α and β parameters could not be distinguished.

Changes in the F_V/F_M and Φ_F (Fig. 2d) measured in the field with the MONI-PAM system also tracked the development of the spring recovery of photosynthesis, rapidly decreasing in response to the two cold spells and gradually recovering from winter to summer. Over the full spring recovery, Φ_F varied approximately by a factor of 2 from its minimum in early April to its maximum in June and July. Variations in F_V/F_M were further decomposed into PQ_S and NPQ_S components (Fig. 2e,f). NPQ_S presented larger seasonal variation decreasing from about 5 at the beginning of the study period to zero during summer. In contrast, PQ_S

increased from values of about 3 at the beginning of the study period to values of 4.5 during summer. Both NPQ_S and PQ_S consistently responded to both cold spells, increasing and decreasing, respectively.

Seasonal changes in pigment content and leaf absorption

No obvious seasonal patterns were observed in total Chl levels (Fig. 3a) although a slightly decreasing trend occurred during spring which reversed towards summer. This result was consistent with the time-series of total leaf PAR absorption ($A_{T(PAR)}$, Fig. S2) which did not display any seasonal pattern either with values ranging from 0.81 to 0.85. In contrast, seasonal changes were observed in Chl b (Fig. 3c), Chl a/b (Fig. 3d), carotenoid content (Fig. 3e) and Car/Chl ratios (Fig. 3f). During early spring, Chl a/b ratios were lower and carotenoid and Car/Chl ratios higher than during summer. No clear effects of the cold spells were seen in the pigments, except for Chl a/b which displayed higher levels after the second cold spell and Car/Chl which had a tendency to increase after the cold spells.

Seasonal variation in ChlF spectra

The ChlF spectra of pine needles measured at room temperature and at standard illumination (F_λ, Fig. 4a-c) was used here as a proxy of variations in the spectrally resolved fluorescence yield. F_λ experienced strong seasonal changes during the study period, mainly in terms of intensity but also in shape. For example, the red peak near 690nm was nearly absent during winter (Fig. 4a,b), but gradually reappeared towards summer (Fig. 4c). Both red (F_{690}) and far-red (F_{740}) ChlF (Fig.

4d) increased from early spring to summer with a larger change in F_{740}. Integrated ChlF ($\int_{660}^{780} F\, d\lambda$, Fig. 4e), used here for comparison with the spectrally averaged Φ_F, presented a similar seasonal pattern with the rest of photosynthetic parameters. Both Φ_F (Fig. 2d) and $\int_{660}^{780} F\, d\lambda$ (Fig. 4e) varied seasonally by a factor of 2. The F_{690}/F_{740} ratio drastically decreased from 0.5 to 0.4 in response to the first cold spell, and did not reverse to 0.5 until several weeks later (Fig. 4f). Later on, the ratio decreased again to about 0.45 by the end of the study period, coinciding with the increase in total Chl (Fig. 3a) and F_λ (Fig. 4d).

Principal component analysis

Three principal components explained 99.8% of the variation in ChlF spectra during the study period (Fig. 5). PC1 explained 98.8% of variance of ChlF spectra across the spring recovery (Fig. 5a) and exhibited a clear and similar seasonal pattern (Fig. 5b) to that of red, far-red, and integrated ChlF (Fig. 4d,e). The spectral weights and intensity of PC1 reflected the shape and seasonal variation in Φ_F. In contrast, PC2 (Fig. 5c) explained only 0.8% of variance but its spectral weights presented a strong and wavelength dependent shape reflecting differences in red and far-red ChlF. PC2 potentially indicates seasonal changes in ChlF reabsorption (i.e. f_{esc} (λ) in Eqn.1), changes in energy redistribution between PSII and PSI, or changes in the emission spectra at the photosystem level. Remarkably, a drastic increase of PC2 (Fig. 5d) was detected upon the first cold spell (solid and vertical black line), and later on during summer when foliar Chl content tended to increase (Fig. 3a). Overall, the seasonal pattern of PC2 closely resembled the mirror image of F_{690}/F_{740} (Fig. 4f). PC3 explained only 0.2%

of variance (Fig. 5e) and displayed no clear seasonal trend other than a sharp decrease at the end of April (Fig. 5f).

Seasonal correlations between photosynthetic parameters and spectral ChlF

Measurements of red, far-red and integral ChlF under standardized conditions were strongly correlated with field photosynthetic parameters α (*r*: 0.81-0.83), β (*r:* 0.84-0.86) and F_V/F_M (*r*: 0.87-0.89) (*P*<0.001 for all; Fig. 6 and Fig. S4). In contrast, no significant relationships between F_{690}/F_{740} and photosynthetic parameters were found. Red (F_{690}) and far-red (F_{740}) ChlF were strongly and negatively correlated also with leaf carotenoid content (*r*: -0.9 and -0.87, respectively) and NPQ_S (*r*: -0.86 and -0.83, respectively), and positively related with Φ_F (*r*: 0.73 and 0.71, respectively) and PQ_S (*r*: 0.74 and 0.71, respectively) (*P*<0.001 for all; Fig. 6 and Fig. S4). In fact, NPQ_S and leaf carotenoid content were the two factors that displayed the strongest (negative) correlation with the spring recovery of photosynthesis in terms of α, β, and F_V/F_M. No significant relationship was observed between red or far-red ChlF and total Chl or $A_{T(PAR)}$ (Fig. S4).

As for the principal components, PC1 was correlated strongly with F_V/F_M (*r* = 0.87), and negatively correlated with carotenoid, Car/Chl, and NPQ_S (*r*: -0.87 to -0.83), and had a significant but slightly lower relationship with Φ_F and PQ_S (*r* = 0.72) (*P*<0.001 for all; Fig. 6 and Fig. S4). PC2 was highly and negatively correlated with F_{690}/F_{740} (*r* = -0.92; *P*<0.001) but was not significantly correlated with $A_{T(PAR)}$ (*r* = 0.51) and total Chl (*r* = 0.37). Finally, PC3 was only marginally correlated with Chl a/b (*r* = 0.45; *P* = 0.06).

We also conducted a systematic assessment of the seasonal correlations between different ChlF emission wavelengths and photosynthetic parameters (Fig. 7). The results indicated that both red and far-red ChlF wavelengths were strongly correlated with the spring recovery of photosynthesis (P<0.001 for all), represented here by the photosynthetic parameters α and β (Fig. 7a), with red wavelengths displaying stronger correlations than far-red wavelengths. Correlations were also stronger for β, compared to α across the whole spectral range, which is not surprising since our spectral measurements were conducted at high light. The strength of the correlation decreased between the two ChlF emission peak, with highest RMSE (data not shown). As expected, a wavelength dependency in the slope of α (β) vs. F_λ was also observed (Fig. 7b), further emphasizing that the ratio LUE/$\Phi_F(\lambda)$ (as in Eqn. 3) was dependent on ChlF emission wavelengths. Positive intercepts of F_λ vs. α (β) (Fig. 7c; with ranges of 0.15 to 0.95 mW m^{-2} sr^{-1} nm^{-1}) were obtained for both parameters and across wavelengths, indicating positive ChlF emission when photosynthetic gas exchange approaches zero.

Additionally, all the main ChlF emission wavelengths from 680 to 770 nm were well correlated with Φ_F (P<0.001 for all), and presented slightly stronger relationships in the red region than far-red (Fig. S5a). This was consistent with better correlations of ChlF with photosynthetic parameters in the red than in the far-red wavelengths (Fig. 7a). Further, when comparing F_λ to $\int_{660}^{780} F\, d\lambda$, red wavelengths presented slightly lower correlations (Fig. S5b), reflecting that red ChlF fluorescence wavelengths account for a source of independent information not conveyed by broadband ChlF.

Discussion

We followed the spectral response of ChlF during the spring recovery of photosynthesis. We found an across wavelength increase in ChlF 'level' well correlated with photosynthetic parameters, and additional subtler changes in spectral shape over time. Critically, photosystems in overwintering evergreens undergo major structural and biochemical adjustments during the non-photosynthetic season (Adams & Demmig-Adams 1994; Ottander *et al.* 1995; Gilmore & Ball 2000; Ensminger *et al.* 2004; Verhoeven 2014), which were reflected in the variation of the measured ChlF spectra.

Seasonal variation in leaf-level ChlF spectra and its controls

We used PCA analysis to separate and quantify the relative roles of different components of variation in the seasonal ChlF dynamics of pine needles. We found that 98.8% of the seasonal variation in ChlF spectra of needles was explained by changes in ChlF level (PC1) with only a marginal 1% of variation associated with additional changes in shape (with PC2 explaining 0.8%). Factors contributing to these components of variation are discussed next.

Lack of correlation between F_{690}, F_{740} (and PC1), and total Chl content or $A_{T(PAR)}$ (Figs. 6 and S4) evidenced the minor role of PAR absorption in driving the seasonality of ChlF during the spring recovery. In the present study Chl content remained relatively stable (Fig. 3a). This is at odds with previous work where significant seasonal changes in Chl content have been observed in Scots pine needles (Ottander *et al.* 1995; Ensminger *et al.* 2004, Porcar-Castell *et al.* 2012), and other evergreen species (Wong & Gamon 2015). It is unclear why we

observed such differences in pigments; but considering the alternative scenario where Chl did change during the season, and as the bulk of the spring recovery of ChlF in Scots pine needles has been shown to precede the summer increase in foliar Chl content by about two weeks (Porcar-Castell *et al.* 2008a), changes in leaf PAR absorption (*A*, Eqn.1) will likely remain of lesser importance in controlling the seasonality in leaf-level SIF(λ) in evergreen conifers. We also did not find evidence of an inverse and persistent relationship between red/far-red ratio and foliar Chl content across the study period (Figs. 6 and S4), as would follow from the general Chl reabsorption theory (Fig. 4A in Gitelson, Buschmann & Lichtenthaler 1999; Fig. 4 in Buschmann 2007). This result demonstrates that, in addition to foliar Chl content, other factors also influence the shape of the ChlF spectra.

Seasonal changes in both F_{690} and F_{740} (and PC1) were strongly related to seasonal variation in foliar carotenoid content, NPQs, and to a lesser extent PQs (Fig. 6). The mechanisms that drive NPQs in overwintering evergreens (understood as the sustained enhancement in the capacity for thermal dissipation of excitation energy), remain under intense investigation (Demmig-Adams & Adams 2006; Verhoeven 2014; Ruban 2016; Malnoë 2018). NPQs in evergreens has been associated to: the accumulation of carotenoids (especially zeaxanthin) relative to Chl (Adams & Demmig-Adams 1994; Ensminger *et al.* 2004; Zarter *et al.* 2006a; Porcar-Castell *et al.* 2012), the accumulation of damaged or non-functional PSII reaction centers coupled to a reduction in the PSII core D1 protein (Ottander *et al.* 1995; Ensminger *et al.* 2004; Ebbert, Adams, Mattoo, Sokolenko & Demmig-Adams 2005), the presence and accumulation of early-light induced proteins (Elips) with or without concomitant changes in minor antenna PsbS

proteins (Ensminger *et al.* 2004; Ebbert *et al.* 2005; Zarter *et al.* 2006b; Verhoeven 2014), the aggregation of light-harvesting complexes of PSII (LHCII) (Horton *et al.* 1991; Ottander *et al.* 1995; Busch, Hüner & Ensminger 2007; Ruban 2018), and the unstacking of the thylakoid membrane (Demmig-Adams *et al.* 2015).

Reversible forms of NPQ, which operate in time scales of seconds to minutes, (e.g. energy-dependent or zeaxanthin-dependent quenching qE and qZ, respectively) (Verhoeven 2014; Malnoë 2018), are known to predominantly quench ChlF associated with PSII units with no apparent effect on PSI ChlF (Genty *et al.* 1990; Franck *et al.* 2002). As a result, because the ChlF contribution from PSI is much larger around the far-red peak (Genty *et al.* 1990; Pfündel 1998; Franck *et al.* 2002), an increase in qE or qZ results in a reduction in the red/far-red ChlF ratio (Agati, Mazzinghi, Fusi & Ambrosini 1995; Agati *et al.* 2000). If the PSI ChlF contribution would be also insensitive to NPQs, we would have expected a similar decrease in F_{690}/F_{740} in response to the seasonal accumulation of NPQs. This scenario was not fully supported by our observations because the extremes of variation in F_{690}/F_{740} ratio (observed during March, Fig. 4f) took place under comparable Chl and NPQs levels (Figs. 2f and 3a), suggesting that PSI ChlF contribution is dynamic at the seasonal scale.

Seasonal changes in the ChlF ratio are clearly driven by multiple controls. For example, F_{690}/F_{740} decreased from 0.5 to 0.4 in response to the first cold spell, along with an increase in NPQs (Fig. 2f) and in PC2 (Fig. 5d) which occurred under rather stable Chl content (Fig. 3a). This phenomena could denote a structural reorganization at the level of LHCII (increased reabsorption due to aggregation), or thylakoid membrane unstacking (promoting energetic

565 connectivity between PSII and PSI units) accompanying the accumulation of
566 NPQs. In fact, similar decreases in red/far-red ChlF ratio have been reported in
567 response to reversible NPQ-induced oligomerization of LHCII complexes
568 (Miloslavina *et al.* 2008; Jahns & Holzwarth 2012). Later on, in mid-May and July
569 we registered a slight increase in foliar Chl content (Fig. 3a) accompanied by a
570 decrease in the F_{690}/F_{740} ratio (Fig. 4f), and under rather stable NPQs (Fig. 2f)
571 corresponding to the previous characterized relationship between leaf Chl
572 content and the ChlF ratio (Gitelson *et al.* 1999). Overall, further experimental
573 and modelling studies are needed to clarify the mechanisms that drive the
574 dynamics in the ChlF spectra in overwintering evergreens.

575

576 *Wavelength dependency between ChlF and photosynthesis*

577 We found that all the main ChlF emission wavelengths (680-770 nm) were
578 correlated with and capable of tracking the photosynthetic spring recovery in
579 boreal evergreen foliage (Fig. 7a). This finding was consistent with the dominant
580 role of NPQs in controlling the seasonal variability in the ChlF level across
581 wavelengths (PC1; Fig. 5a,b). It is important to note however that the relative
582 contributions of the variation in spectral shape (1% for PC2+PC3) and ChlF level
583 (98.8% for PC1) to total seasonal variation in ChlF spectral properties could have
584 been very different in a different species or under a different set of environmental
585 conditions, encouraging further seasonal studies across other species and
586 biomes.

587 Slightly higher correlations (Fig. 7a) and slopes (Fig. 7b) were found between red
588 wavelengths of F_λ and α and β. Similar results have been reported at the canopy
589 scale based on model simulations (Verrelst *et al.* 2015; Liu *et al.* 2019) and

experimental data (Cheng *et al.* 2013; Campbell *et al.* 2019; Magney *et al.* 2019a). At the leaf-level, the higher correlation in red wavelengths could point to interferences with the dynamics or PSI ChlF in the far-red wavelengths. In fact, the spectral shape of the intercept (Fig. 7c), which represents the background ChlF spectra at zero photosynthesis, had a high resemblance to the typical spectral shape of PSI ChlF, although the peak was slightly red-shifted (740 nm) compared to earlier studies in non-downregulated leaves of barley (722 nm) (Franck *et al.* 2002) or maize PSI particles (725-730 nm) (Croce, Dorra, Holzwarth & Jennings 2000). Further work to characterize and identify the drivers of this background ChlF signal, which may have important implications for interpretation of SIF data over boreal evergreen regions, is needed.

Implications at the larger scale

SIF is a promising methodology for the estimation of GPP dynamics in terrestrial ecosystems either using statistical methods based on Eqn. 3 (Guanter *et al.* 2014; Sun *et al.* 2017; Li *et al.* 2018), or by assimilation into the photosynthetic modules of land surface models (Lee *et al.* 2015; Thum *et al.* 2017; Macbean *et al.* 2018). SIF could be particularly useful for evergreen ecosystems by capturing part of the temporal dynamics of GPP that remains hidden to traditional reflectance-based vegetation indices due to low variation in greenness (Walther *et al.* 2016; Smith *et al.* 2018; Zuromski *et al.* 2018; Magney *et al.* 2019a; Nichol *et al.* 2019).

Overall, our results indicate that current Fraunhofer- and oxygen-based methods to retrieve SIF across different wavelengths in the red and near-infrared regions (Meroni *et al.* 2009; Lu, Cheng, Li & Tang 2018) have similar intrinsic potential to capture the leaf-level spring recovery of photosynthesis in boreal evergreen

615 forests. Importantly, when upscaling from the leaf to the canopy and landscape
616 level, the constancy assumption behind the $LUE/\Phi_F(\lambda)$ factor in Eqn. 3 will be
617 further complicated by spatial variation in physiological factors caused by within
618 canopy light and temperature gradients or species composition (Porcar-Castell
619 *et al.* 2014; Sun *et al.* 2017). Similarly, canopy-level f_{esc} (Eqn. 3) will be also
620 affected by seasonal dynamics in canopy structure related to the phenology of
621 the multiple components in the ecosystem, including the understory (Majasalmi,
622 Stenberg & Rautiainen 2017; Liu *et al.* 2019).

623

624 **Conclusions**

625 We demonstrated that red and far-red ChlF emission wavelengths were able to
626 transmit the optical signature of the spring recovery of photosynthesis in boreal
627 evergreen needles. The dynamics of the spectral signature were mediated by the
628 complex and highly articulated process of sustained regulatory thermal
629 dissipation or NPQ_S, which effectively quenches all ChlF wavelengths. Although
630 changes in the shape of the ChlF spectra explained only a marginal proportion of
631 the observed seasonality, the information content embedded in these changes
632 could be highly informative. Specifically, the rapid decrease in the F_{690}/F_{740} ratio
633 upon the first cold spell suggests that in addition to Chl content, F_{690}/F_{740} can also
634 convey information on the structural organization in the thylakoid membrane in
635 overwintering evergreens, which could help to better constrain the assimilation of
636 SIF data into models of photosynthesis (Macbean *et al.* 2018; Raczka *et al.* 2019).
637 Further investigations across species and scales will be required to fully
638 characterize the information potentially embedded in the spectral dynamics of SIF,
639 in support of multispectral SIF retrievals from towers, drones, airplanes as well

as satellite missions such as current TROPOspheric Monitoring Instrument, TROPOMI, onboard Sentinel-5 (Guanter *et al.* 2015; Köhler *et al.* 2018) or future Fluorescence Explorer mission, FLEX (Drusch *et al.* 2017).

Acknowledgements: We acknowledge the financial support from the Academy of Finland (288039, 293443, 319211, 272041), the COST Action ES1309/OPTIMISE, the European Research Council Synergy grant SyG-2013-610028 IMBALANCE-P, the Spanish Government project CGL2016-79835-P, the Catalan Government project SGR 2014-274, and the Funds from the University of Helsinki (Grant 490116). HR was supported by EU LIFE 12 ENV/FI/000409 Monimet. CZ gratefully acknowledges the support from the China Scholarship Council.

Conflict of interest: The authors have no conflicts of interest to declare.

Author Contribution: Albert Porcar-Castell, Jon Atherton, Iolanda Filella, Josep Peñuelas and Jaana Bäck conceived and designed the study; Chao Zhang and Albert Porcar-Castell carried out the optical measurements; Chao Zhang and Jon Atherton conducted the majority of the data analysis; Pasi Kolari estimated the photosynthetic parameters; Juho Aalto carried out and processed the field gas exchange data at SMEAR-II station; Hanna Ruhanen conducted the pigments analysis; Chao Zhang and Albert Porcar-Castell wrote the paper with contributions from all authors.

664 **References**

665 Aalto J., Kolari P., Hari P., Kerminen V.M., Schiestl-Aalto P., Aaltonen H., …
666 Bäck J. (2014) New foliage growth is a significant, unaccounted source for
667 volatiles in boreal evergreen forests. *Biogeosciences* **11**, 1331–1344.

668 Adams W.W. & Demmig-Adams B. (1994) Carotenoid composition and down
669 regulation of photosystem II in three conifer species during the winter.
670 *Physiologia Plantarum* **92**, 451–458.

671 Agati G., Cerovic Z.G. & Moya I. (2000) The effect of decreasing temperature
672 up to chilling values on the in vivo F685/F735 chlorophyll fluorescence ratio
673 in *Phaseolus vulgaris* and *Pisum sativum*: the role of the photosystem I
674 contribution to the 735 nm fluorescence band. *Photochemistry and*
675 *Photobiology* **72**, 75–84.

676 Agati G., Mazzinghi P., Fusi F. & Ambrosini I. (1995) The F685/F730 chlorophyll
677 fluorescence ratio as a tool in plant physiology: response to physiological
678 and environmental factors. *Journal of Plant Physiology* **145**, 228–238.

679 Alonso L., Gómez-chova L., Vila-francés J., Amorós-lópez J., Guanter L., Calpe
680 J. & Moreno J. (2007) Sensitivity analysis of the Fraunhofer Line
681 Discrimination method for the measurement of chlorophyll fluorescence
682 using a field spectroradiometer. *IEEE*, 3756–3759.

683 Baker N.R. (2008) Chlorophyll fluorescence: a probe of photosynthesis *in vivo*.
684 *Annual review of plant biology* **59**, 89–113.

685 Barber J., Malkin S. & Telfer A. (1989) The origin of chlorophyll fluorescence *in*
686 *vivo* and its quenching by the photosystem II reaction centre. *Philosophical*
687 *Transactions of the Royal Society B: Biological Sciences* **323**, 227–239.

688 Busch F., Hüner N.P.A. & Ensminger I. (2007) Increased air temperature during
689 simulated autumn conditions does not increase photosynthetic carbon gain
690 but affects the dissipation of excess energy in seedlings of the evergreen
691 conifer jack pine. *Plant Physiology* **143**, 1242–1251.

692 Buschmann C. (2007) Variability and application of the chlorophyll fluorescence
693 emission ratio red/far-red of leaves. *Photosynthesis Research* **92**, 261–271.

694 Campbell P.K., Huemmrich K.F., Middleton E.M., Ward L.A., Julitta T., Daughtry
695 C.S., … Kustas W.P. (2019) Diurnal and seasonal variations in chlorophyll
696 fluorescence associated with photosynthesis at leaf and canopy scales.
697 *Remote Sensing* **11**, 1–36.

698 Cheng Y., Middleton E.M., Zhang Q., Huemmrich K.F., Campbell P.K.E., Corp
699 L.A., … Daughtry C.S. (2013) Integrating solar induced fluorescence and
700 the photochemical reflectance index for estimating gross primary
701 production in a cornfield. *Remote Sensing* **5**, 6857–6879.

702 Croce R., Dorra D., Holzwarth A.R. & Jennings R.C. (2000) Fluorescence decay
703 and spectral evolution in intact photosystem I of higher plants. *Biochemistry*
704 **39**, 6341–6348.

705 Damm A., Guanter L., Paul-limoges E., Tol C. Van Der, Hueni A., Buchmann
706 N., … Schaepman M.E. (2015) Far-red sun-induced chlorophyll
707 fluorescence shows ecosystem-specific relationships to gross primary
708 production: An assessment based on observational and modeling
709 approaches. *Remote Sensing of Environment* **166**, 91–105.

710 Demmig-Adams B. & Adams W.W. (2006) Photoprotection in an ecological
711 context: the remarkable complexity of thermal energy dissipation. *New*

712 *Phytologist* **172**, 11–21.

713 Demmig-Adams B., Muller O., Stewart J.J., Cohu C.M. & Adams W.W. (2015)
714 Chloroplast thylakoid structure in evergreen leaves employing strong
715 thermal energy dissipation. *Journal of Photochemistry and Photobiology B:*
716 *Biology* **152**, 357–366.

717 Drusch M., Moreno J., Del Bello U., Franco R., Goulas Y., Huth A., … Verhoef
718 W. (2017) The FLuorescence EXplorer Mission Concept-ESA's Earth
719 Explorer 8. *IEEE Transactions on Geoscience and Remote Sensing* **55**,
720 1273–1284.

721 Ebbert V., Adams W.W., Mattoo A.K., Sokolenko A. & Demmig-Adams B.
722 (2005) Up-regulation of a photosystem II core protein phosphatase inhibitor
723 and sustained D1 phosphorylation in zeaxanthin-retaining, photoinhibited
724 needles of overwintering Douglas fir. *Plant, Cell and Environment* **28**, 232–
725 240.

726 Ensminger I., Sveshnikov D., Campbell D.A.., Funk C., Jansson S., Lloyd J., …
727 Öquist G. (2004) Intermittent low temperatures constrain spring recovery of
728 photosynthesis in boreal Scots pine forests. *Global Change Biology* **10**,
729 995–1008.

730 Franck F., Juneau P. & Popovic R. (2002) Resolution of the Photosystem I and
731 Photosystem II contributions to chlorophyll fluorescence of intact leaves at
732 room temperature. *Biochimica et Biophysica Acta - Bioenergetics* **1556**,
733 239–246.

734 Frankenberg C. & Berry J. (2018) Solar induced chlorophyll fluorescence :
735 origins , relation to photosynthesis and retrieval. In *Reference Module in*

736 *Earth Systems and Environmental Sciences: Comprehensive Remote*
737 *Sensing, Elsevier, Oxford*. pp. 143–162. Elsevier.

738 Frankenberg C., Fisher J.B., Worden J., Badgley G., Saatchi S.S., Lee J.E., …
739 Yokota T. (2011) New global observations of the terrestrial carbon cycle
740 from GOSAT: Patterns of plant fluorescence with gross primary
741 productivity. *Geophysical Research Letters* **38**, 1–6.

742 Frankenberg C., O'Dell C., Berry J., Guanter L., Joiner J., Köhler P., … Taylor
743 T.E. (2014) Prospects for chlorophyll fluorescence remote sensing from the
744 Orbiting Carbon Observatory-2. *Remote Sensing of Environment* **147**, 1–
745 12.

746 Genty B., Wonders J. & Baker N.R. (1990) Non-photochemical quenching of F_o
747 in leaves is emission wavelength dependent: consequences for quenching
748 analysis and its interpretation. *Photosynthesis Research* **26**, 133–139.

749 Gilmore A.M. & Ball M.C. (2000) Protection and storage of chlorophyll in
750 overwintering evergreens. *Proceedings of the National Academy of*
751 *Sciences* **97**, 11098–11101.

752 Gitelson A.A., Buschmann C. & Lichtenthaler H.K. (1999) The chlorophyll
753 fluorescence ratio F_{735} / F_{700} as an accurate measure of the chlorophyll
754 content in plants. *Remote Sensing of Environment* **69**, 296–302.

755 Govindjee G. (1995) Sixty-three years since Kautsky: chlorophyll *a*
756 fluorescence. *Australian Journal of Plant Physiology* **22**, 131–160.

757 Guanter L., Aben I., Tol P., Krijger J.M., Hollstein A., Köhler P., … Landgraf J.
758 (2015) Potential of the TROPOspheric Monitoring Instrument (TROPOMI)
759 onboard the Sentinel-5 Precursor for the monitoring of terrestrial chlorophyll

760 fluorescence. *Atmospheric Measurement Techniques* **8**, 1337–1352.

761 Guanter L., Zhang Y., Jung M., Joiner J., Voigt M., Berry J.A., … Moran M.S.
762 (2014) Global and time-resolved monitoring of crop photosynthesis with
763 chlorophyll fluorescence. *Proceedings of the National Academy of*
764 *Sciences*, 1–7.

765 Hari P. & Kulmala M. (2005) Station for measuring ecosystem-atmosphere
766 relations (SMEAR II). *Boreal Environment Research* **10**, 351–322.

767 Hari P., Mäkelä A., Korpilahti E. & Holmberg M. (1986) Optimal control of gas
768 exchange. *Tree Physiology* **2**, 169–175.

769 Horton P., Ruban A. V., Rees D., Pascal A.A., Noctor G. & Young A.J. (1991)
770 Control of the light-harvesting function of chloroplast membranes by
771 aggregation of the LHCII chlorophyll-protein complex. *FEBS Letters* **292**,
772 1–4.

773 Huang W., Yang Y.J., Hu H. & Zhang S.B. (2016) Seasonal variations in
774 photosystem I compared with photosystem II of three alpine evergreen
775 broad-leaf tree species. *Journal of Photochemistry and Photobiology B:*
776 *Biology* **165**, 71–79.

777 Idle D.B. & Proctor C.W. (1983) An integrating sphere leaf chamber. *Plant, Cell*
778 *and Environment* **6**, 437–439.

779 IPCC-SR15 (2018) *Special report IPCC. "Global Warming of 1.5°C."*

780 Jahns P. & Holzwarth A.R. (2012) The role of the xanthophyll cycle and of lutein
781 in photoprotection of photosystem II. *Biochimica et Biophysica Acta -*
782 *Bioenergetics* **1817**, 182–193.

783 Joiner J., Yoshida Y., Guanter L. & Middleton E.M. (2016) New methods for the
784 retrieval of chlorophyll red fluorescence from hyperspectral satellite
785 instruments: simulations and application to GOME-2 and SCIAMACHY.
786 *Atmospheric Measurement Techniques* **9**, 3939–3967.

787 Kitajima M. & Butler W.L. (1975) Quenching of chlorophyll fluorescence and
788 primary photochemistry in chloroplasts by dibromothymoquinone.
789 *Biochimica et Biophysica Acta* **376**, 105–115.

790 Köhler P., Frankenberg C., Magney T.S., Guanter L., Joiner J. & Landgraf J.
791 (2018) Global retrievals of solar-induced chlorophyll fluorescence with
792 TROPOMI: first results and intersensor comparison to OCO-2. *Geophysical*
793 *Research Letters* **45**, 10,456-10,463.

794 Kolari P., Bäck J., Taipale R., Ruuskanen T.M., Kajos M.K., Rinne J., … Hari P.
795 (2012) Evaluation of accuracy in measurements of VOC emissions with
796 dynamic chamber system. *Atmospheric Environment* **62**, 344–351.

797 Kolari P., Chan T., Porcar-Castell A., Bäck J., Nikinmaa E. & Juurola E. (2014)
798 Field and controlled environment measurements show strong seasonal
799 acclimation in photosynthesis and respiration potential in boreal Scots pine.
800 *Frontiers in Plant Science* **5**, 717.

801 Kolari P., Lappalainen H.K., Hänninen H. & Hari P. (2007) Relationship between
802 temperature and the seasonal course of photosynthesis in Scots pine at
803 northern timberline and in southern boreal zone. *Tellus B: Chemical and*
804 *Physical Meteorology* **59B**, 542–552.

805 Lee J.-E., Berry J.A., van der Tol C., Yang X., Guanter L., Damm A., …
806 Frankenberg C. (2015) Simulations of chlorophyll fluorescence

807 incorporated into the Community Land Model version 4. *Global Change*
808 *Biology* **21**, 3469–3477.

809 Li X., Xiao J., He B., Arain M.A., Beringer J., Desai A.R., … Varlagin A. (2018)
810 Solar-induced chlorophyll fluorescence is strongly correlated with terrestrial
811 photosynthesis for a wide variety of biomes: First global analysis based on
812 OCO-2 and flux tower observations. *Global Change Biology*, 1–19.

813 Liu W., Atherton J., Mõttus M., Gastellu-Etchegorry J.P., Malenovský Z.,
814 Raumonen P., … Porcar-Castell A. (2019) Simulating solar-induced
815 chlorophyll fluorescence in a boreal forest stand reconstructed from
816 terrestrial laser scanning measurements. *Remote Sensing of Environment*
817 **in press**.

818 Lu X., Cheng X., Li X. & Tang J. (2018) Opportunities and challenges of
819 applications of satellite-derived sun-induced fluorescence at relatively high
820 spatial resolution. *Science of the Total Environment* **619**–**620**, 649–653.

821 Macbean N., Maignan F., Bacour C., Lewis P., Guanter L., Köhler P., … Disney
822 M. (2018) Strong constraint on modelled global carbon uptake using solar-
823 induced chlorophyll fluorescence data. *Scientific reports*, 1–12.

824 Magney T.S., Bowling D.R., Logan B., Grossmann K., Stutz J., Blanken P., …
825 Frankenberg C. (2019a) Mechanistic evidence for tracking the seasonality
826 of photosynthesis with solar-induced fluorescence. *Proceedings of the*
827 *National Academy of Sciences* **116**, 11640–11645.

828 Magney T.S., Frankenberg C., Köhler P., North G., Davis T.S., Dold C., …
829 Porcar-Castell A. (2019b) Disentangling changes in the spectral shape of
830 chlorophyll fluorescence: Implications for remote sensing of

photosynthesis. *Journal of Geophysical Research: Biogeosciences* **124**, 1–17.

Majasalmi T., Stenberg P. & Rautiainen M. (2017) Comparison of ground and satellite-based methods for estimating stand-level fPAR in a boreal forest. *Agricultural and Forest Meteorology* **232**, 422–432.

Malnoë A. (2018) Photoinhibition or photoprotection of photosynthesis? Update on the (newly termed) sustained quenching component qH. *Environmental and Experimental Botany* **154**, 123–133.

Meroni M., Rossini M., Guanter L., Alonso L., Rascher U., Colombo R. & Moreno J. (2009) Remote sensing of solar-induced chlorophyll fluorescence: review of methods and applications. *Remote Sensing of Environment* **113**, 2037–2051.

Migliavacca M., Perez-Priego O., Rossini M., El-Madany T.S., Moreno G., van der Tol C., … Reichstein M. (2017) Plant functional traits and canopy structure control the relationship between photosynthetic CO_2 uptake and far-red sun-induced fluorescence in a Mediterranean grassland under different nutrient availability. *New Phytologist* **214**, 1078–1091.

Miloslavina Y., Wehner A., Lambrev P.H., Wientjes E., Reus M., Garab G., … Holzwarth A.R. (2008) Far-red fluorescence: A direct spectroscopic marker for LHCII oligomer formation in non-photochemical quenching. *FEBS Letters* **582**, 3625–3631.

Monteith J.L. (1972) Solar radiation and productivity in tropical ecosystems. *Journal of Applied Ecology* **9**, 747–766.

Murata N., Takahashi S., Nishiyama Y. & Allakhverdiev S.I. (2007)

855 Photoinhibition of photosystem II under environmental stress. *Biochimica et*
856 *Biophysica Acta - Bioenergetics* **1767**, 414–421.

857 Murchie E.H. & Lawson T. (2013) Chlorophyll fluorescence analysis: a guide to
858 good practice and understanding some new applications. *Journal of*
859 *Experimental Botany* **64**, 3983–3998.

860 Nichol C., Drolet G., Porcar-Castell A., Wade T., Sabater N., Middleton E., …
861 Atherton J. (2019) Seasonal solar induced chlorophyll fluorescence and
862 photosynthesis in a boreal Scots pine canopy. *Remote Sensing* **11**, 273.

863 Olascoaga B., Mac Arthur A., Atherton J. & Porcar-Castell A. (2016) A
864 comparison of methods to estimate photosynthetic light absorption in
865 leaves with contrasting morphology. *Tree Physiology* **36**, 368–379.

866 Öquist G., Chow W.S. & Anderson J.M. (1992) Photoinhibition of
867 photosynthesis represents a mechanism for the long-term regulation of
868 photosystem II. *Planta* **186**, 450–460.

869 Öquist G., Hällgren J.E. & Brunes L. (1978) An apparatus for measuring
870 photosynthetic quantum yields and quanta absorption spectra of intact
871 plants. *Plant, Cell and Environment* **1**, 21–27.

872 Öquist G. & Huner N.P.A. (2003) Photosynthesis of overwintering evergreen
873 plants. *Annual Review of Plant Biology* **54**, 329–355.

874 Ottander C., Campbell D. & Öquist G. (1995) Seasonal changes in photosystem
875 II organisation and pigment composition in *Pinus sylvestris*. *Planta* **197**,
876 176–183.

877 Ottander C. & Öquist G. (1991) Recovery of photosynthesis in winter-stressed
878 Scots pine. *Plant, Cell and Environment* **14**, 345–349.

879 Palombi L., Cecchi G., Lognoli D., Raimondi V., Toci G. & Agati G. (2011) A
880 retrieval algorithm to evaluate the photosystem I and photosystem II
881 spectral contributions to leaf chlorophyll fluorescence at physiological
882 temperatures. *Photosynthesis research* **108**, 225–239.

883 Parazoo N.C., Arneth A., Pugh T.A.M., Smith B., Steiner N., Luus K., … Miller
884 C. (2018) Spring photosynthetic onset and net CO_2 uptake in Alaska
885 triggered by landscape thawing. *Global Change Biology*, 3416–3435.

886 Parazoo N.C., Bowman K., Fisher J.B., Frankenberg C., Jones D.B.A., Cescatti
887 A., … Montagnani L. (2014) Terrestrial gross primary production inferred
888 from satellite fluorescence and vegetation models. *Global Change Biology*
889 **20**, 3103–3121.

890 Pfündel E. (1998) Estimating the contribution of photosystem I to leaf
891 chlorophyll fluorescence. *Photosynthesis Research* **56**, 185–195.

892 Pfündel E.E., Klughammer C., Meister A. & Cerovic Z.G. (2013) Deriving
893 fluorometer-specific values of relative PSI fluorescence intensity from
894 quenching of F_0 fluorescence in leaves of *Arabidopsis thaliana* and *Zea*
895 *mays*. *Photosynthesis research* **114**, 189–206.

896 Pirinen P., Simola H., Aalto J., Kaukoranta J.-P., Karlsson P. & Ruuhela R.
897 (2012) *Tilastoja suomen ilmastosta 1981-2010. (Climatological statistics of*
898 *Finland 1981–2010)*.

899 Porcar-Castell A. (2011) A high-resolution portrait of the annual dynamics of
900 photochemical and non-photochemical quenching in needles of *Pinus*
901 *sylvestris*. *Physiologia Plantarum* **143**, 139–153.

902 Porcar-Castell A., Mac Arthur A., Rossini M., Eklundh L., Pacheco-Labrador J.,

903 Anderson K., … Vescovo L. (2015) EUROSPEC: At the interface between
904 remote-sensing and ecosystem CO_2 flux measurements in Europe.
905 *Biogeosciences* **12**, 6103–6124.

906 Porcar-Castell A., Garcia-Plazaola J.I., Nichol C.J., Kolari P., Olascoaga B.,
907 Kuusinen N., … Nikinmaa E. (2012) Physiology of the seasonal relationship
908 between the photochemical reflectance index and photosynthetic light use
909 efficiency. *Oecologia* **170**, 313–323.

910 Porcar-Castell A., Juurola E., Ensminger I., Berninger F., Hari P. & Nikinmaa E.
911 (2008a) Seasonal acclimation of photosystem II in *Pinus sylvestris*. II.
912 Using the rate constants of sustained thermal energy dissipation and
913 photochemistry to study the effect of the light environment. *Tree physiology*
914 **28**, 1483–1491.

915 Porcar-Castell A., Pfündel E., Korhonen J.F.J. & Juurola E. (2008b) A new
916 monitoring PAM fluorometer (MONI-PAM) to study the short- and long-
917 term acclimation of photosystem II in field conditions. *Photosynthesis*
918 *research* **96**, 173–179.

919 Porcar-Castell A., Tyystjärvi E., Atherton J., van der Tol C., Flexas J., Pfündel
920 E.E., … Berry J.A. (2014) Linking chlorophyll a fluorescence to
921 photosynthesis for remote sensing applications: mechanisms and
922 challenges. *Journal of Experimental Botany* **65**, 4065–4095.

923 Quéré C. Le, Andrew R.M., Friedlingstein P., Sitch S., Hauck J., Pongratz J., …
924 Adrie and B.Z. (2018) Global Carbon Budget 2018. *Earth System Science*
925 *Data* **10**, 2141–2194.

926 Raczka B., Porcar-Castell A., Magney T., Lee J.E., Köhler P., Frankenberg

927 C., … Bowling D.R. (2019) Sustained non-photochemical quenching
928 shapes the seasonal pattern of solar-induced fluorescence at a high-
929 elevation evergreen forest. *Journal of Geophysical Research:*
930 *Biogeosciences* **124**.

931 Rajewicz P., Atherton J., Alonso L. & Porcar-Castell A. (2019) Leaf-level
932 spectral fluorescence measurements: comparing methodologies for
933 broadleaves and needles. *Remote Sensing* **11**, 1–20.

934 Rascher U., Alonso L., Burkart A., Cilia C., Cogliati S., Colombo R., … Zemek
935 F. (2015) Sun-induced fluorescence – a new probe of photosynthesis: First
936 maps from the imaging spectrometer *HyPlant*. *Global Change Biology* **21**,
937 4673–4684.

938 Romero J.M., Cordon G.B. & Lagorio M.G. (2018) Modeling re-absorption of
939 fluorescence from the leaf to the canopy level. *Remote Sensing of*
940 *Environment* **204**, 138–146.

941 Ruban A. V. (2018) Light harvesting control in plants. *FEBS Letters* **592**, 3030–
942 3039.

943 Ruban A. V (2016) Nonphotochemical chlorophyll fluorescence quenching:
944 mechanism and effectiveness in protecting plants from photodamage. *Plant*
945 *physiology* **170**, 1903–1916.

946 Ruban A. V, Johnson M.P. & Duffy C.D.P. (2012) The photoprotective
947 molecular switch in the photosystem II antenna. *Biochimica et Biophysica*
948 *Acta* **1817**, 167–181.

949 Smith P., Bustamante M., Ahammad H., Clark H., Dong H., Elsiddig E.A., …
950 Tubiello F.N. (2014) Agriculture, Forestry and Other Land Use (AFOLU).

951 *Climate Change 2014: Mitigation of Climate Change. Contribution of*
952 *Working Group III to the Fifth Assessment Report of the Intergovernmental*
953 *Panel on Climate Change*, 811–922.

954 Smith W.K., Biederman J.A., Scott R.L., Moore D.J.P., He M., Kimball J.S., …
955 Litvak M.E. (2018) Chlorophyll fluorescence better captures seasonal and
956 interannual gross primary productivity dynamics across dryland
957 ecosystems of southwestern North America. *Geophysical Research Letters*
958 **45**, 748–757.

959 Sonoike K. (2011) Photoinhibition of Photosystem I. *Physiologia Plantarum* **142**,
960 56–64.

961 Soukupová J., Cséfalvay L., Urban O., Košvancová M., Marek M., Rascher U. &
962 Nedbal L. (2008) Annual variation of the steady-state chlorophyll
963 fluorescence emission of evergreen plants in temperate zone. *Functional*
964 *Plant Biology* **35**, 63–76.

965 Springer K.R., Wang R. & Gamon J.A. (2017) Seasonal patterns of
966 photosynthesis, fluorescence, and reflectance indices in boreal trees.
967 *Remote Sensing* **9**, 1–18.

968 Sun Y., Frankenberg C., Jung M., Joiner J., Guanter L., Köhler P. & Magney T.
969 (2018) Overview of Solar-Induced chlorophyll Fluorescence (SIF) from the
970 Orbiting Carbon Observatory-2: Retrieval, cross-mission comparison, and
971 global monitoring for GPP. *Remote Sensing of Environment* **209**, 808–823.

972 Sun Y., Frankenberg C., Wood J.D., Schimel D.S., Jung M., Guanter L., …
973 Yuen K. (2017) OCO-2 advances photosynthesis observation from space
974 via solar-induced chlorophyll fluorescence. *Science* **358**.

975 Thum T., Zaehle S., Köhler P., Aalto T., Aurela M., Guanter L., … Markkanen T.
976 (2017) Modelling sun-induced fluorescence and photosynthesis with a land
977 surface model at local and regional scales in northern Europe.
978 *Biogeosciences* **14**, 1969–1987.

979 van der Tol C., Berry J.A., Campbell P.K.E. & Rascher U. (2014) Models of
980 fluorescence and photosynthesis for interpreting measurements of solar-
981 induced chlorophyll fluorescence. *Journal of Geophysical Research:*
982 *Biogeosciences* **119**, 2312–2327.

983 Verhoeven A. (2014) Sustained energy dissipation in winter evergreens. *New*
984 *Phytologist* **201**, 57–65.

985 Verrelst J., Rivera J.P., van der Tol C., Magnani F., Mohammed G. & Moreno J.
986 (2015) Global sensitivity analysis of the SCOPE model: What drives
987 simulated canopy-leaving sun-induced fluorescence? *Remote Sensing of*
988 *Environment* **166**, 8–21.

989 Verrelst J., van der Tol C., Magnani F., Sabater N., Rivera J.P., Mohammed G.
990 & Moreno J. (2016) Evaluating the predictive power of sun-induced
991 chlorophyll fluorescence to estimate net photosynthesis of vegetation
992 canopies: a SCOPE modeling study. *Remote Sensing of Environment* **176**,
993 139–151.

994 Walther S., Voigt M., Thum T., Gonsamo A., Zhang Y., Kohler P., … Guanter L.
995 (2016) Satellite chlorophyll fluorescence measurements reveal large-scale
996 decoupling of photosynthesis and greenness dynamics in boreal evergreen
997 forests. *Global Change Biology* **22**, 2979–2996.

998 Wellburn A.R. (1994) Spectral determination of chlorophylls a and b, as well as

total carotenoids, using various solvents with spectrophotometers of different resolution. *Journal of Plant Physiology* **144**, 307–313.

Wieneke S., Burkart A., Cendrero-Mateo M.P., Julitta T., Rossini M., Schickling A., … Rascher U. (2018) Linking photosynthesis and sun-induced fluorescence at sub-daily to seasonal scales. *Remote Sensing of Environment* **219**, 247–258.

Van Wittenberghe S., Alonso L., Verrelst J., Moreno J. & Samson R. (2015) Bidirectional sun-induced chlorophyll fluorescence emission is influenced by leaf structure and light scattering properties - A bottom-up approach. *Remote Sensing of Environment* **158**, 169–179.

Wong C.Y.S. & Gamon J.A. (2015) The photochemical reflectance index provides an optical indicator of spring photosynthetic activation in evergreen conifers. *New Phytologist* **206**, 196–208.

Yang P. & van der Tol C. (2018) Linking canopy scattering of far-red sun-induced chlorophyll fluorescence with reflectance. *Remote Sensing of Environment* **209**, 456–467.

Yang P., van der Tol C., Verhoef W., Damm A., Schickling A., Kraska T., … Rascher U. (2018) Using reflectance to explain vegetation biochemical and structural effects on sun-induced chlorophyll fluorescence. *Remote Sensing of Environment*.

Zarco-Tejada P.J., Catalina A., González M.R. & Martín P. (2013) Relationships between net photosynthesis and steady-state chlorophyll fluorescence retrieved from airborne hyperspectral imagery. *Remote Sensing of Environment* **136**, 247–258.

1023 Zarco-Tejada P.J., González-Dugo M. V. & Fereres E. (2016) Seasonal stability
1024 of chlorophyll fluorescence quantified from airborne hyperspectral imagery
1025 as an indicator of net photosynthesis in the context of precision agriculture.
1026 *Remote Sensing of Environment* **179**, 89–103.

1027 Zarter C.R., Adams W.W., Ebbert V., Cuthbertson D.J., Adamska I. & Demmig-
1028 Adams B. (2006a) Winter down-regulation of intrinsic photosynthetic
1029 capacity coupled with up-regulation of Elip-like proteins and persistent
1030 energy dissipation in a subalpine forest. *New Phytologist* **172**, 272–282.

1031 Zarter C.R., Demmig-Adams B., Ebbert V., Adamska I. & Adams W.W. (2006b)
1032 Photosynthetic capacity and light harvesting efficiency during the winter-to-
1033 spring transition in subalpine conifers. *New Phytologist* **172**, 283–292.

1034 Zhang Y., Guanter L., Joiner J., Song L. & Guan K. (2018) Spatially-explicit
1035 monitoring of crop photosynthetic capacity through the use of space-based
1036 chlorophyll fluorescence data. *Remote Sensing of Environment* **210**, 362–
1037 374.

1038 Zuromski L.M., Bowling D.R., Köhler P., Frankenberg C., Goulden M.L.,
1039 Blanken P.D. & Lin J.C. (2018) Solar-induced fluorescence detects
1040 interannual variation in gross primary production of coniferous forests in the
1041 western United States. *Geophysical Research Letters* **45**, 7184–7193.

1042

Figure legends:

Fig. 1. Measurement rationale during the spring recovery of 2015 in *Pinus sylvestris*.

Fig. 2. Seasonal variation of meteorological and photosynthetic parameters.

Fig. 3. Seasonal variation of foliar pigment content.

Fig. 4. Seasonal variation in spectral chlorophyll fluorescence (ChlF).

Fig. 5. Principal component analysis (PCA) for spectral chlorophyll fluorescence.

Fig. 6. Pearson correlation (*r*) matrix between key study variables.

Fig.7. The linear regression between individual spectral fluorescence from 660 to 780 nm (F_λ) and photosynthetic parameters (α and β).

Supporting Information

Figure legends:

Fig. S1. Seasonal changes in CO_2 flux, α, β, α_n, and β_n, for each individual chamber.

Fig. S2. Seasonal variation of leaf total PAR absorption ($A_{T(PAR)}$).

Fig. S3. Linear regression correlations of field F_V/F_M (FMS-2) with field F_V/F_M (MONI-PAM) and lab F_V/F_M (FMS-2).

Fig. S4. The significance matrix of Pearson correlation (*P*) between key study variables.

Fig. S5. Coefficients of determination of the linear regression of individual spectral ChlF with Φ_F and integral spectral ChlF ($\int_{660}^{780} F\ d\lambda$).

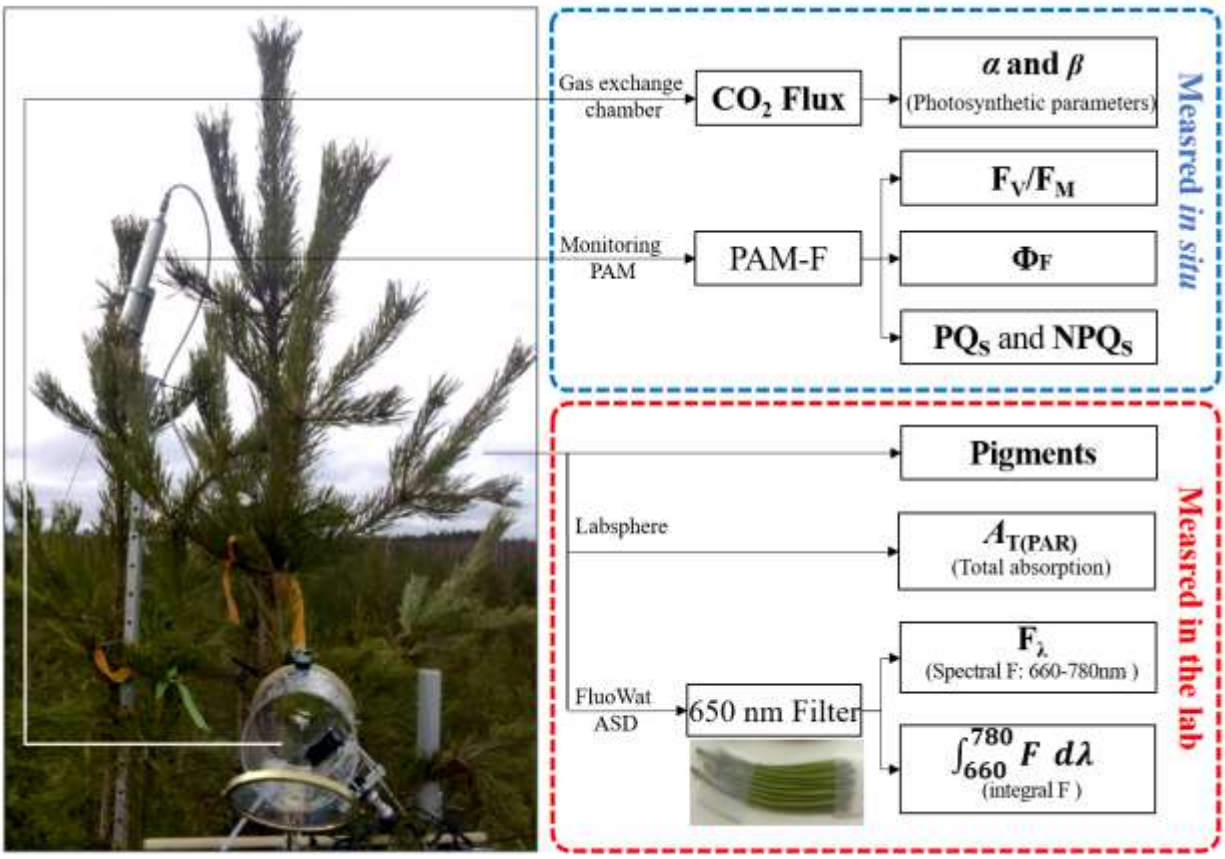

Figure 1. Measurement rationale during the spring recovery of 2015 in *Pinus sylvestris*. *In situ* measurements encompassed (1) continuous gas exchange measurements with automated chambers (N=2-4 trees) to estimate CO_2 flux and derive the seasonal photosynthetic parameters α and β, and (2) continuous PAM fluorescence measurements (N=4) to derive maximum quantum yield of PSII (F_V/F_M), quantum yield of fluorescence (Φ_F), and sustained photochemical (PQ_S) and non-photochemical quenching (NPQ_S). For the lab measurement, needles from top branches (N=5) were sampled during each measuring day. (1) One portion was immediately frozen in liquid nitrogen for posterior pigments analysis. (2) Another portion was rapidly brought to the laboratory, and used to measure total PAR absorption ($A_{T(PAR)}$) and spectral fluorescence (F_λ) respectively (see also Materials and methods section for details).

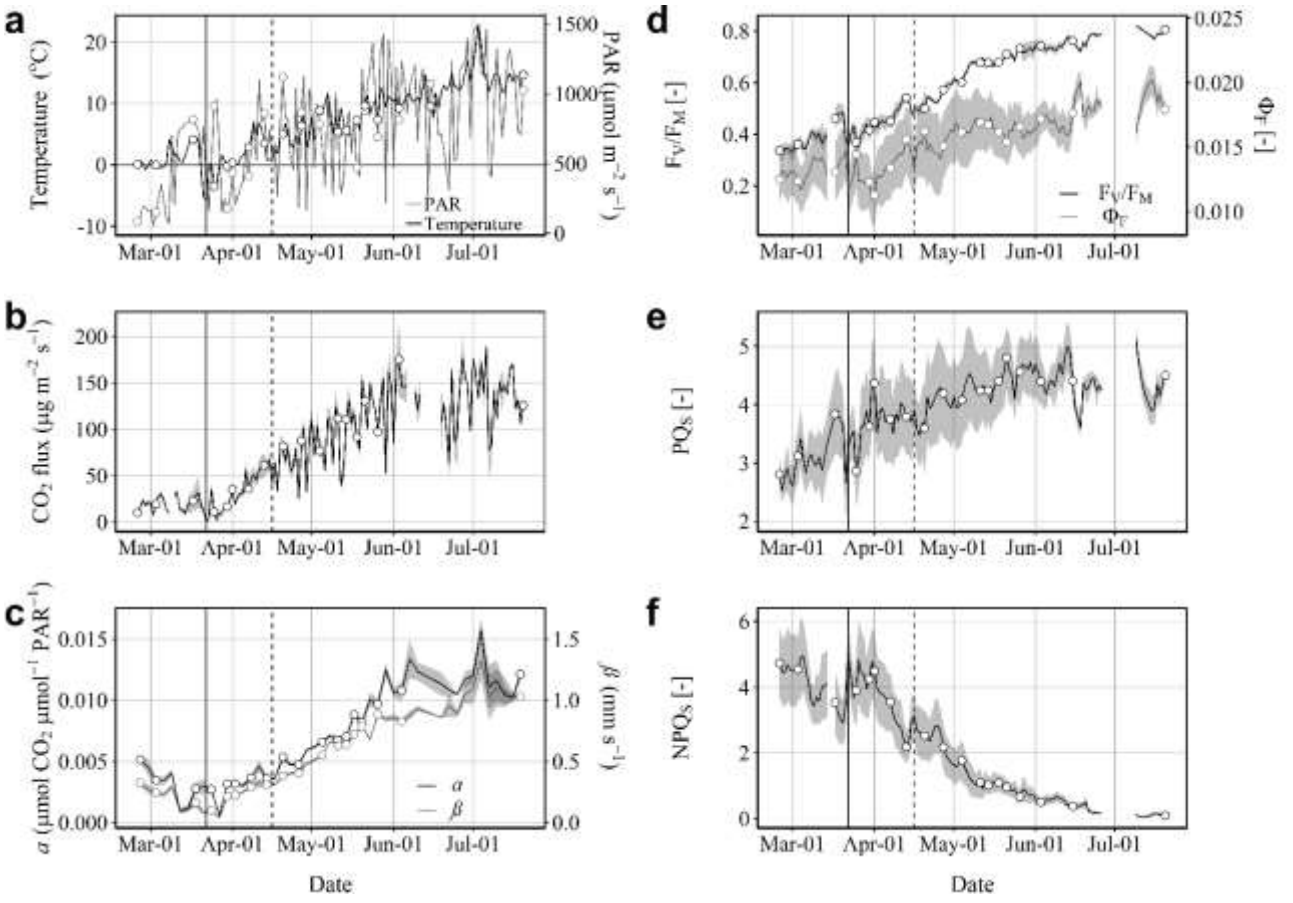

Figure 2. Seasonal variation of meteorological and photosynthetic parameters. (a) Daily mean temperature (°C; *black line*) and mean midday photosynthetically active radiation between 11:00 and 14:00 (PAR; μmol m^{-2} s^{-1}; *grey line*), (b) mean midday CO_2 flux between 11:00 and 14:00 (μg m^{-2} s^{-1}), (c) proxies of maximum photosynthetic light-use efficiency (*α*, *black line*) and maximum photosynthetic rate (*β*, *grey line*) in prevailing conditions estimated from the gas exchange data, (d) daily maximum quantum yield of PSII (F_V/F_M, *black line*) and quantum yield of fluorescence (Φ_F, *grey line*), and (e) sustained photochemical (PQ_S) and (f) non-photochemical (NPQ_S) quenching measured using MONI-PAM. Lines indicate the continuous measurement. Open points represent the dates when sampling took place. Solid black line indicates the first cold spell on March 22nd, and dotted black line indicates the second cold spell on April 16th. Points in b-f represent means of four biological replicates (N = 4). Shadows represent ±SE.

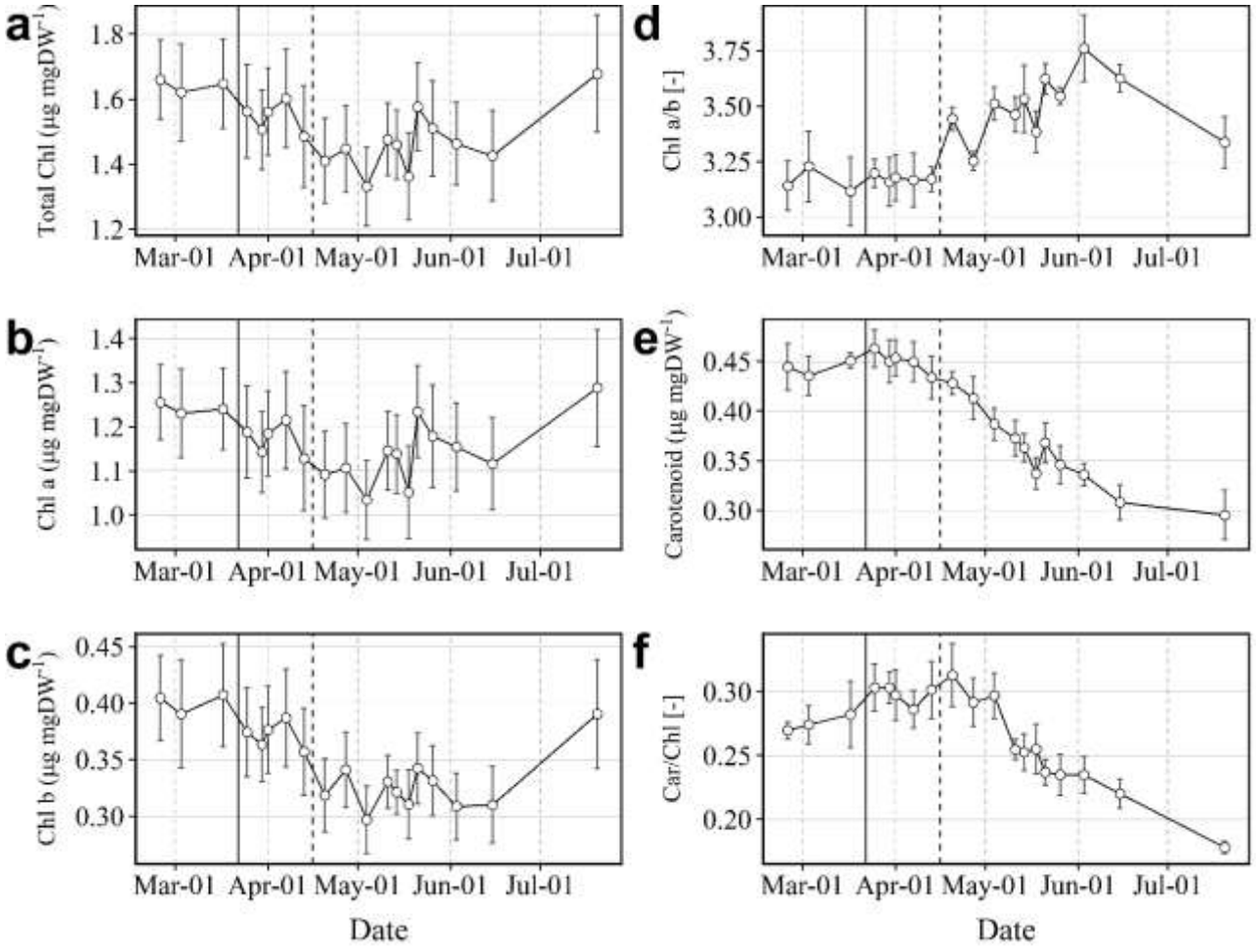

Figure 3. Seasonal variation of foliar pigment content. (a) Total chlorophyll (Chl; µg mgDW^{-1}), (b) Chlorophyll a (Chl a; µg mgDW^{-1}), (c) Chlorophyll b (Chl b; µg mgDW^{-1}), (d) Chlorophyll a / Chlorophyll b (Chl a/b), (e) Total carotenoid (µg mgDW^{-1}), and (f) Carotenoid/Chlorophyll ratio (Car/Chl). Solid black line indicates the first cold spell on March 22nd, and the dotted black line indicates the second cold spell on April 16th. Points represent means of five biological replicates (N = 5). Error bars represent ±SE.

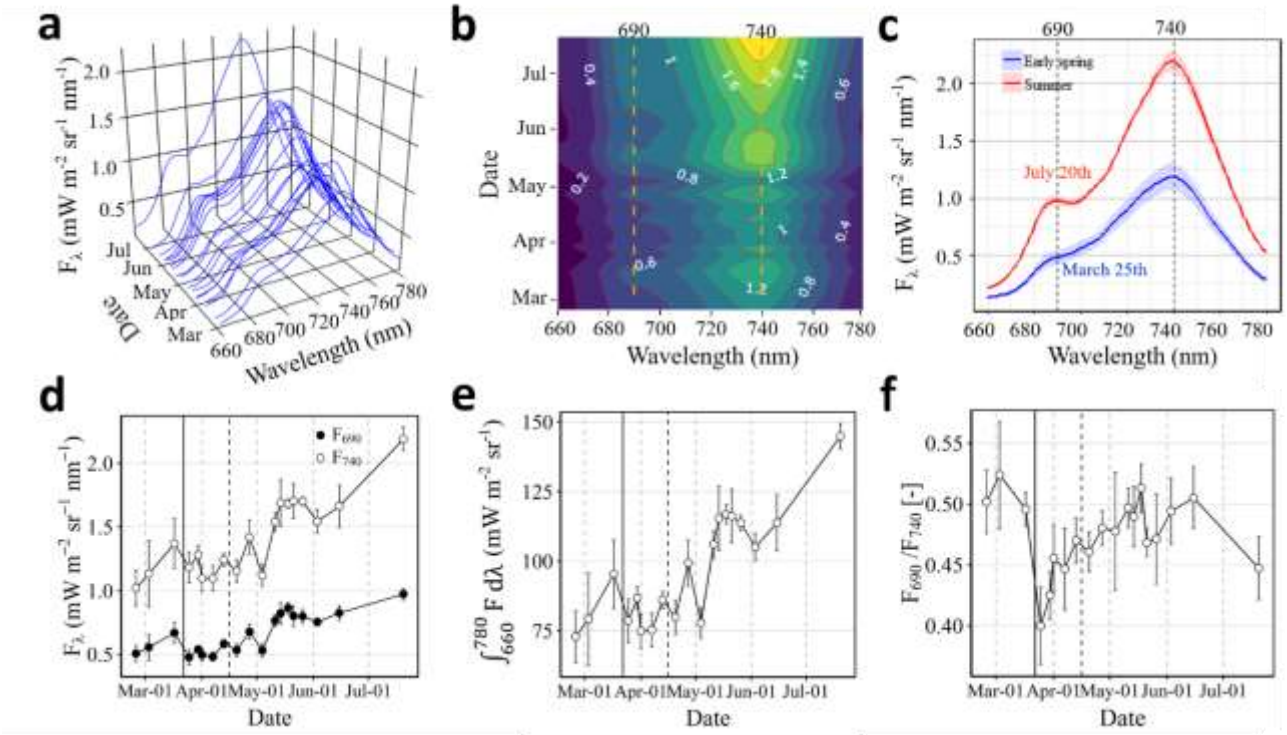

Figure 4. Seasonal variation of spectral chlorophyll fluorescence (ChlF). (a-c) The shape of spectral ChlF from 680 to 770nm (F_λ; mW m^{-2} sr^{-1} nm^{-1}). The contour figure of (b) indicates the F_λ values. Two examples of spectral ChlF in (c) were measured on March 25th (early spring), and July 20th (summer). (d) Red ChlF at 690 nm (F_{690}, *filled circles*) and far-red ChlF at 740 nm (F_{740}, *open circles*), (e) integral ChlF from 660 to 780nm ($\int_{660}^{780} F\, d\lambda$), and (f) fluorescence ratio (F_{690}/F_{740}). Solid and vertical black line indicates the first cold spell on March 22nd, and the dotted and vertical black line indicates the second cold spell on April 16th. Shadows in c and error bars in d-f represent ±SE (N=5).

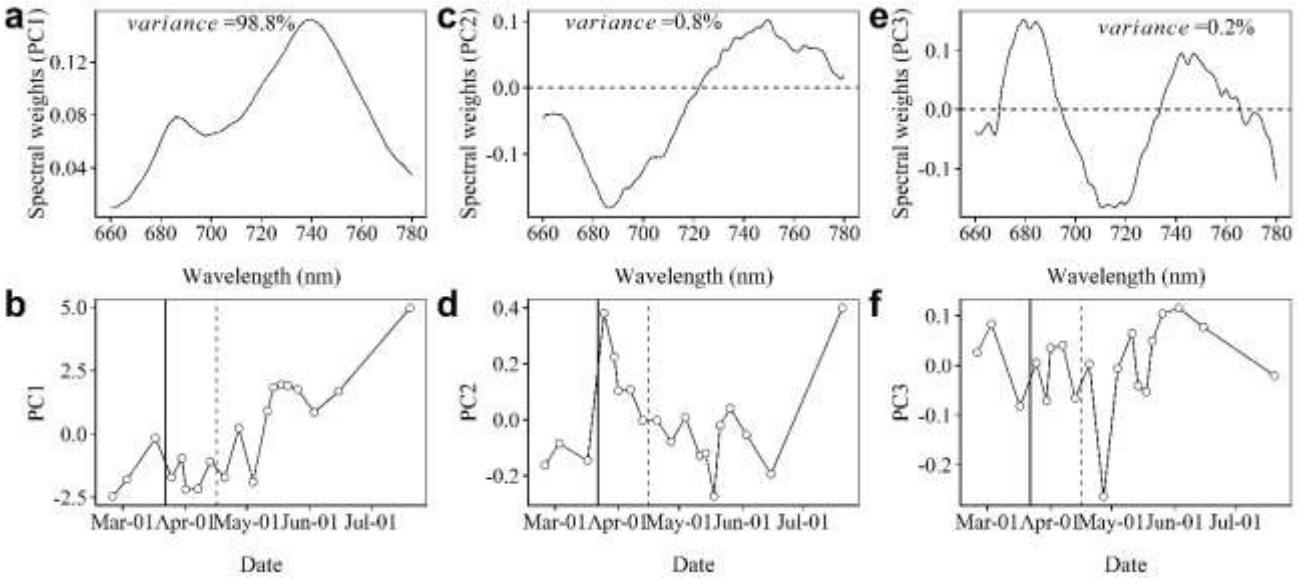

Figure 5. Principal component analysis (PCA) for spectral chlorophyll fluorescence. Panels indicate spectral variability (*top panels*) and seasonal patterns (*bottom panels*) of PC1 (a,b), PC2 (c,d) and PC3 (e,f) respectively. Solid and vertical black line indicates the first cold spell on March 22nd, and dotted and vertical black line indicates the second cold spell on April 16th.

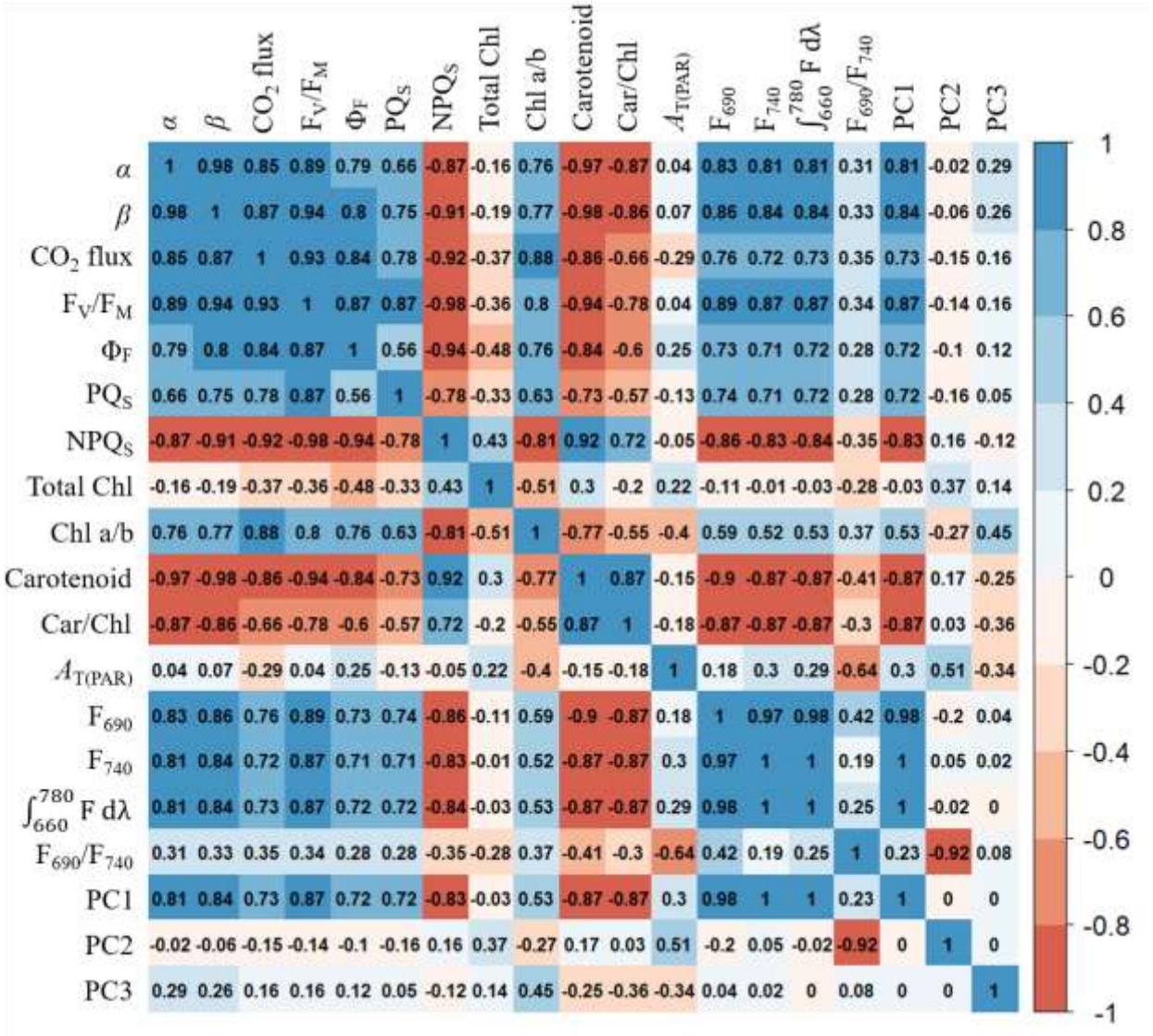

Figure 6. Pearson correlation (*r*) matrix between key study variables. The *r* value is indicated as colour (positive correlations are shaded blue, and negative correlations are shaded orange) and number.

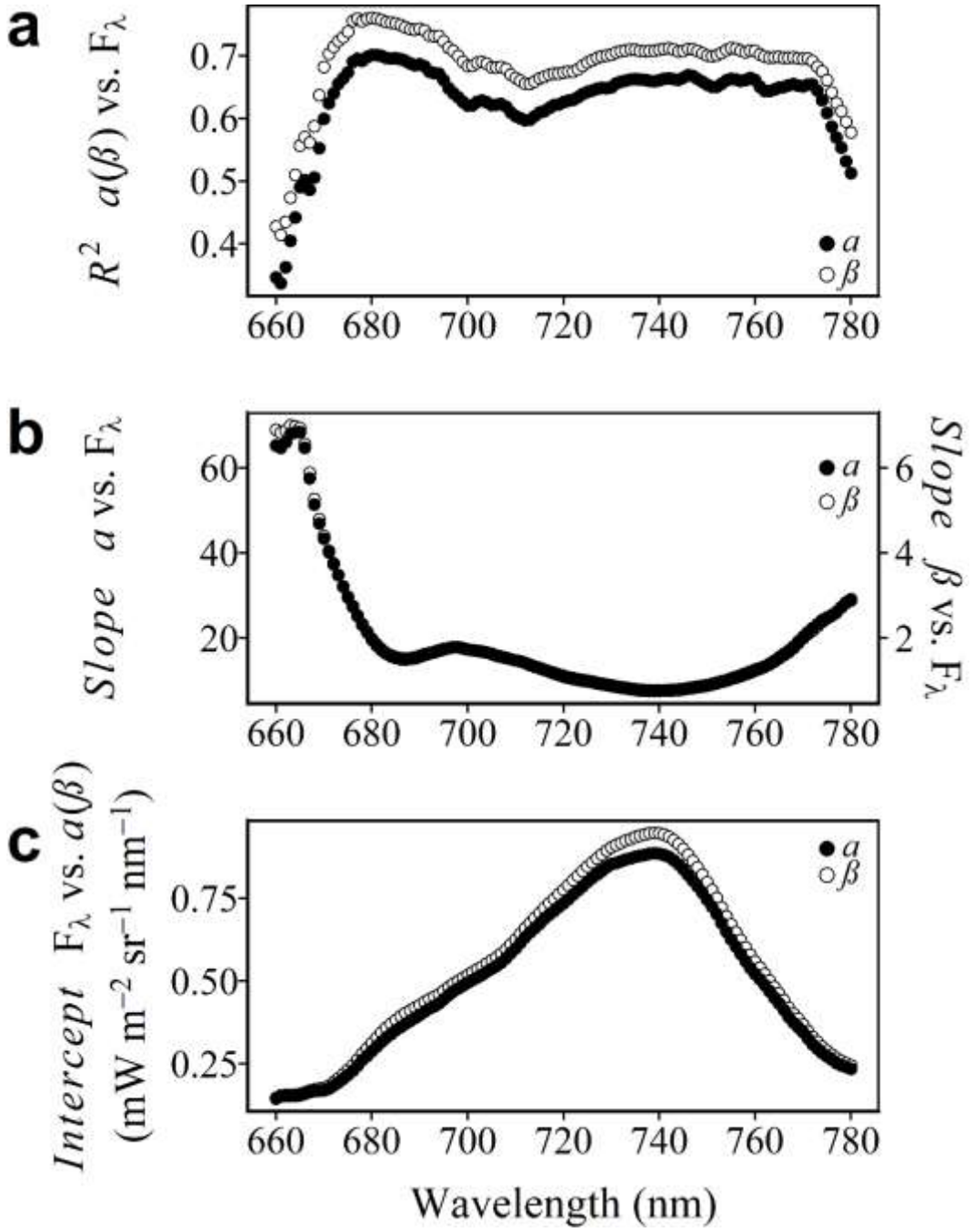

Figure 7. The linear regression between individual spectral fluorescence from 660 to 780 nm (F_λ) and photosynthetic parameters (α, *filled circles* and β, *open circles*). (a) Coefficients of determination (R^2), (b) *slopes* of α (β) vs. F_λ, (c) *intercepts* of F_λ vs. α (β).

Supporting Information of

Do all chlorophyll fluorescence emission wavelengths capture the spring recovery of photosynthesis in boreal evergreen foliage?

Running title: Spectral fluorescence in evergreens

Chao Zhang[1, 2, 3, *], Jon Atherton[1], Josep Peñuelas[2, 3], Iolanda Filella[2, 3], Pasi Kolari[4], Juho Aalto[4, 5], Hanna Ruhanen[6], Jaana Bäck[7], Albert Porcar-Castell[1, *]

Figure legends:

Fig. S1. Seasonal changes in CO_2 flux, α, β, α_n, and β_n, for each individual chamber.

Fig. S2. Seasonal variation of leaf total PAR absorption ($A_{T(PAR)}$).

Fig. S3. Linear regression correlations of field F_V/F_M (FMS-2) with field F_V/F_M (MONI-PAM) and lab F_V/F_M (FMS-2).

Fig. S4. The significance matrix of Pearson correlation (*P*) between key study variables.

Fig. S5. Coefficients of determination of the linear regression of individual spectral ChlF with Φ_F and integral spectral ChlF ($\int_{660}^{780} F\ d\lambda$).

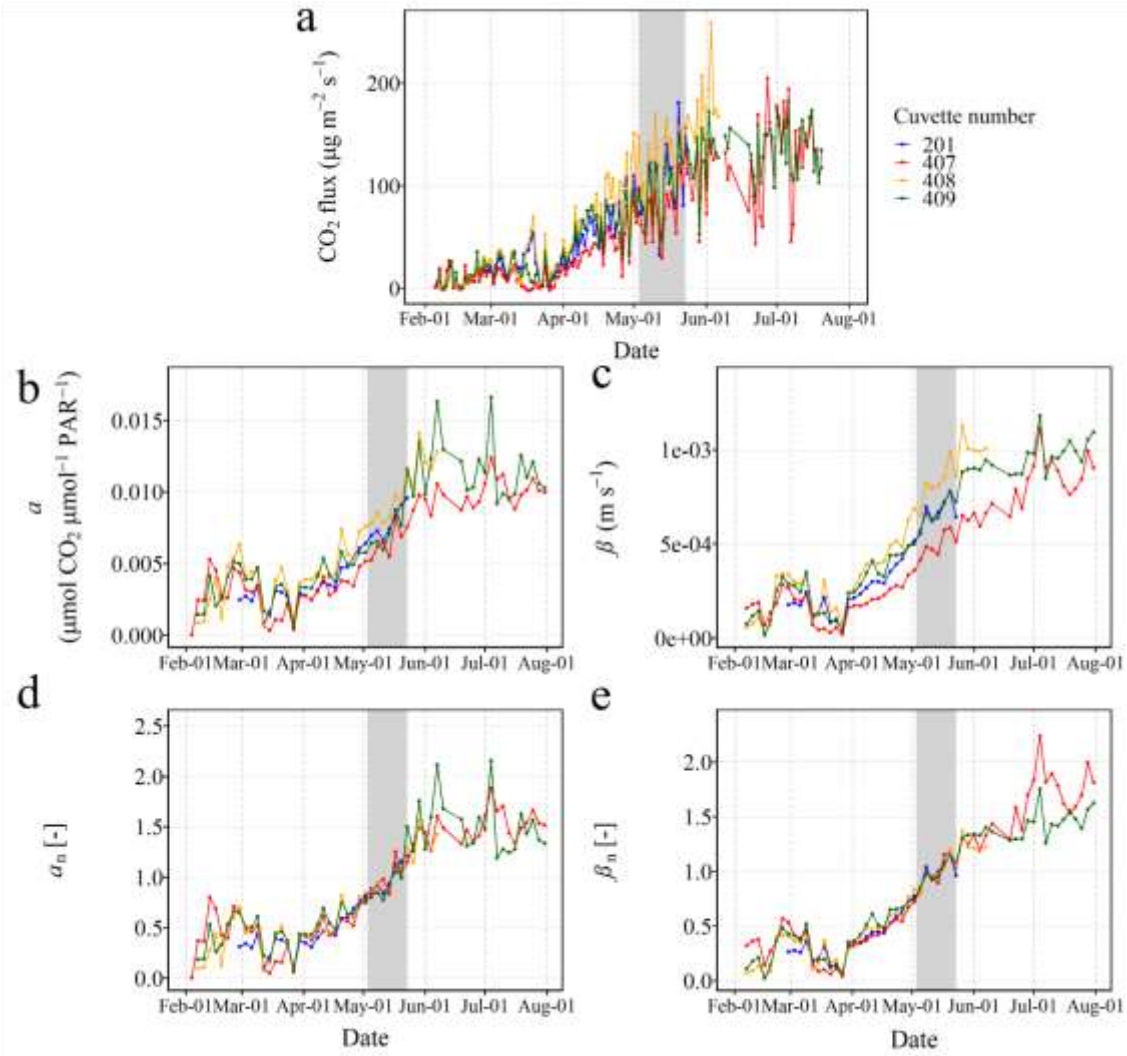

Figure S1. Seasonal changes in (a) CO_2 flux, (b) maximum photosynthetic light-use efficiency parameter α, (c) maximum photosynthetic rate parameter β, (d) normalized α or α_n, and (e) normalized β *or* β_n, for each individual chamber. Note the different temporal coverage for chambers. The grey shadow indicates the period used for the normalization.

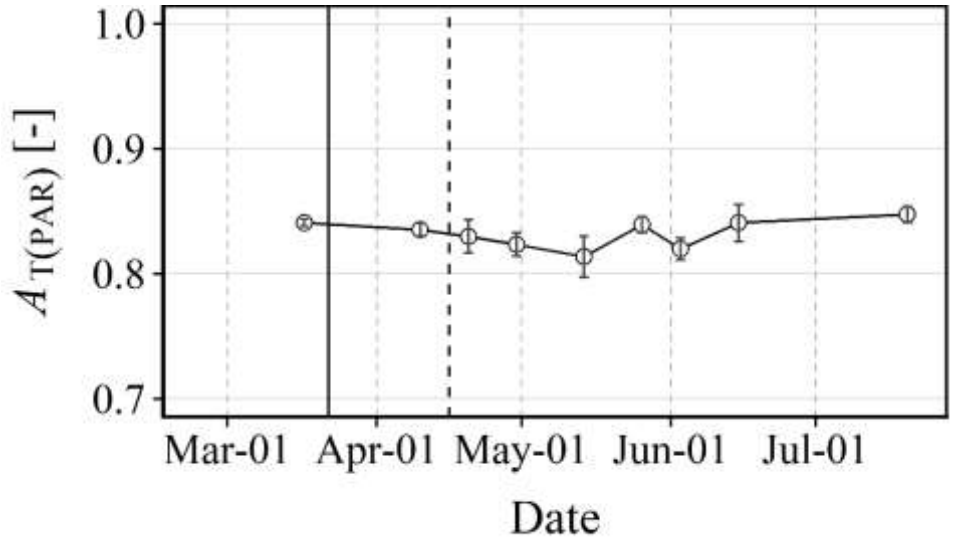

Figure S2. Seasonal variation of leaf total PAR absorption ($A_{T(PAR)}$). Solid and vertical black line indicates the first cold spell on March 22nd, and the dotted and vertical black line indicates the second cold spell on April 16th. Points represent means of five biological replicates (N = 5). Grey error bars represent ±SE.

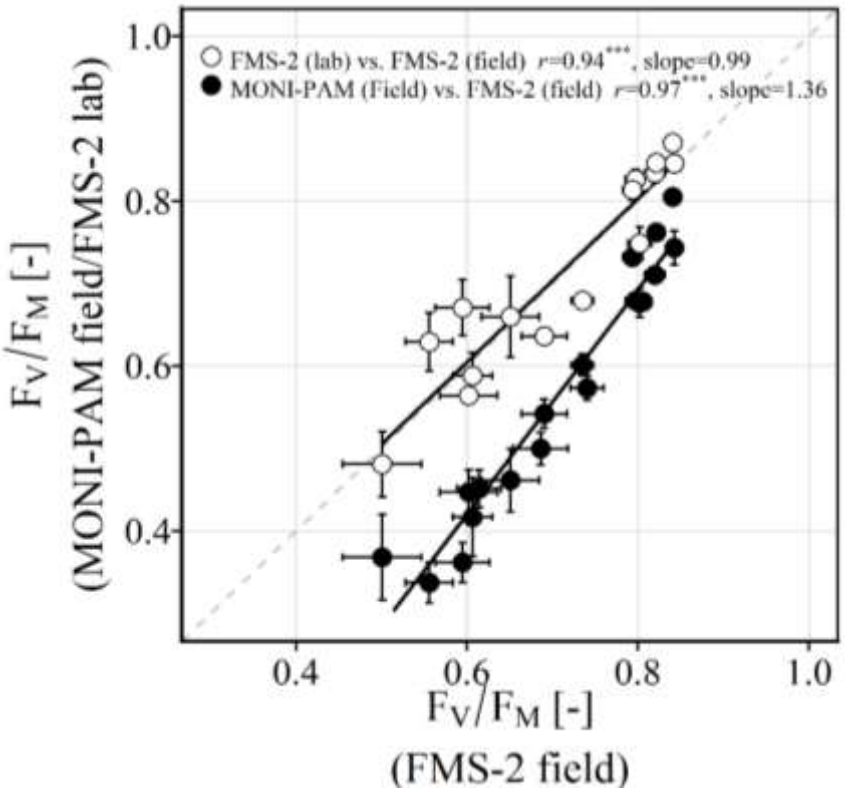

Figure S3. Linear regression correlations of F_V/F_M measured in the field using FMS-2 with F_V/F_M measured using MONI-PAM in the field (*filled circles*) and using FMS-2 in the lab (*open circles*). Points represent means of four (*filled circles*) or five (*open circles*) biological replicates (N = 4 or 5). Dotted grey line is 1:1 line. ****P*<0.001. Error bars represent ±SE (N = 4 or 5).

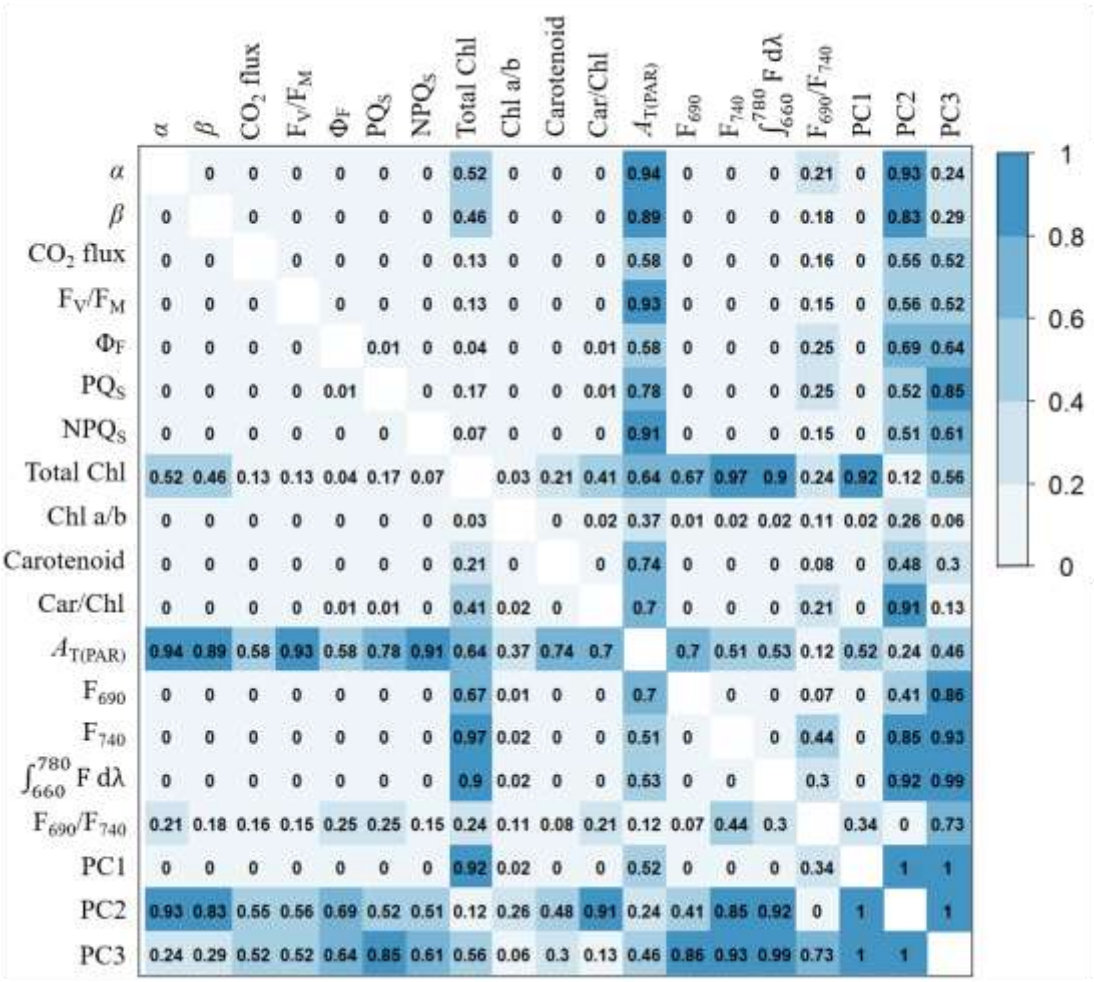

Figure S4. The significance matrix of Pearson correlation (*P*) between key study variables. The *P* value is indicated as colour and number.

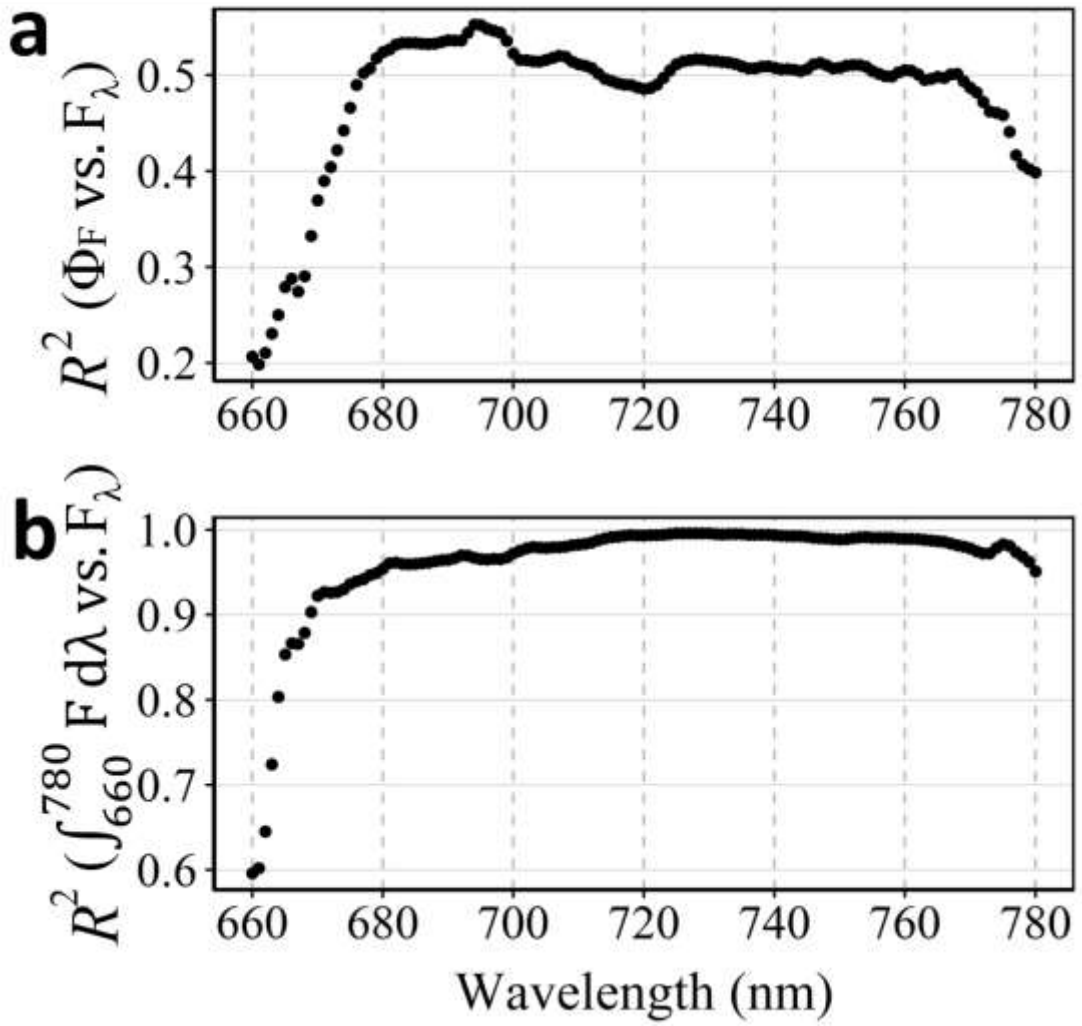

Figure S5. Coefficients of determination (R^2) of the linear regression of individual spectral fluorescence (F_λ) with (a) PAM-based fluorescence yield (Φ_F) and (b) integral spectral ChlF from 660 to 780nm ($\int_{660}^{780} F\, d\lambda$